Meteoritics & Planetary Science 39, Nr 7, 1145–1167 (2004)
Abstract available online at http://meteoritics.org

Secondary alteration of the impactite and mineralization in the basal Tertiary sequence, Yaxcopoil-1, Chicxulub impact crater, Mexico

Doreen E. AMES,[1*] Ingrid M. KJARSGAARD,[2] Kevin O. POPE,[3]
Burkhard DRESSLER,[4] and Mark PILKINGTON[1]

[1]Natural Resources Canada, Geological Survey of Canada, 601 Booth Street, Ottawa, Ontario, K1A 0E8, Canada
[2]Mineralogical Consultant, 15 Scotia Place, Ottawa, Ontario, K1S 0W2, Canada
[3]Geo Eco Arc Research, 16305 St Mary's Church Road, Aquasco, Maryland 20608, USA
[4]Lunar and Planetary Science Institute, Houston, Texas 77058, USA
*Corresponding author. E-mail: dames@nrcan.gc.ca

(Received 30 September 2003; revision accepted 22 February 2004)

Abstract–The 65 Ma Chicxulub impact crater formed in the shallow coastal marine shelf of the Yucatán Platform in Mexico. Impacts into water-rich environments provide heat and geological structures that generate and focus sub-seafloor convective hydrothermal systems. Core from the Yaxcopoil-1 (Yax-1) hole, drilled by the Chicxulub Scientific Drilling Project (CSDP), allowed testing for the presence of an impact-induced hydrothermal system by: a) characterizing the secondary alteration of the 100 m-thick impactite sequence; and b) testing for a chemical input into the lower Tertiary sediments that would reflect aquagene hydrothermal plume deposition. Interaction of the Yax-1 impactites with seawater is evident through redeposition of the suevites (unit 1), secondary alteration mineral assemblages, and the subaqueous depositional environment for the lower Tertiary carbonates immediately overlying the impactites.

The least-altered silicate melt composition intersected in Yax-1 is that of a calc-alkaline basaltic andesite with 53.4–56 wt% $SiO_{2\ (\text{volatile-free})}$. The primary mineralogy consists of fine microlites of diopside, plagioclase (mainly Ab 47), ternary feldspar (Ab 37 to 77), and trace apatite, titanite, and zircon. The overprinting alteration mineral assemblage is characterized by Mg-saponite, K-montmorillonite, celadonite, K-feldspar, albite, Fe-oxides, and late Ca and Mg carbonates. Mg and K metasomatism resulted from seawater interaction with the suevitic rocks producing smectite-K-feldspar assemblages in the absence of any mixed layer clay minerals, illite, or chlorite. Rare pyrite, sphalerite, galena, and chalcopyrite occur near the base of the impactites. These secondary alteration minerals formed by low temperature (0–150 °C) oxidation and fixation of alkalis due to the interaction of glass-rich suevite with down-welling seawater in the outer annular trough intersected at Yax-1. The alteration represents a cold, Mg-K-rich seawater recharge zone, possibly recharging higher temperature hydrothermal activity proposed in the central impact basin. Hydrothermal metal input into the Tertiary ocean is shown by elevated Ni, Ag, Au, Bi, and Te concentrations in marcasite and Cd and Ga in sphalerite in the basal 25 m of the Tertiary carbonates in Yax-1. The lower Tertiary trace element signature reflects hydrothermal metal remobilization from a mafic source rock and is indicative of hydrothermal venting of evolved seawater into the Tertiary ocean from an impact-generated hydrothermal convective system.

INTRODUCTION

Impact-generated hydrothermal systems are common for impact craters developed on shelf environments (i.e. Sudbury: Ames et al. 1998; Kara: Naumov 2002). This is simply due to the heat provided through impact processes initiating sub-seafloor circulation of seawater within the crater. Heat sources available to drive a convective hydrothermal system in an impact environment include the central uplift (e.g.. Manson et al. 1996; Puchezh-Katunki; Naumov 2002), the melt sheet (Sudbury; Ames et al. 1998), and the inherent heat in the impact brecciated basement rocks (e.g. Ivanov and Deutsch 1999). Seawater, groundwater, deep-formational brines and magmatic fluids from the melt sheet are the fluid sources recognized at other impact sites (McCarville and Crossey 1996; Ames et al. 1998; Farrow and Watkinson 1999; Molnar et al. 2001; Ames 2002). The circulation of fluids is controlled by the permeable impactites, syn-crater faults and paleotopography (Ames et al. 2000). Convective circulation of fluids through impacted crustal sequences can influence the heat transfer and cooling of the impact sequences, affect the source of magnetic anomalies, influence the type and location of mineralization, and influence density, porosity, and seismic velocity through precipitation of secondary minerals. Mineralogical and magnetic studies have identified a hydrothermal system within the Chicxulub crater, but its temporal and spatial extent is, as yet, unknown (Schuraytz et al. 1994; Steiner 1996; Pilkington and Hildebrand 2000). Pilkington and Hildebrand (2000) defined two concentric zones of enhanced magnetization. These coincide with the edge of the central uplift at a radius of ~20 km and the edge of the collapsed disruption cavity at a radius of ~45 km (Fig. 1). The distribution and character of the magnetic anomalies were interpreted to be the result of an impact-induced hydrothermal system at Chicxulub. A study of the secondary alteration associated with these magnetic signatures may play a significant role in unravelling the petrogenesis of the melt, and the geophysical signature and mineral potential of the deeply buried crater.

Hydrothermal fluids discharged from vents on the modern seafloor mix with ambient seawater and spread laterally for tens to thousands of km (Baker et al. 1995). Chemical precipitants from the overlying water column have distinctive, zoned trace element signatures relative to the vent location and can form in seafloor volcanic, sedimentary (Spry et al. 2000), and impact crater environments (Whitehead et al. 1992; Ames et al. 2002). The hydrothermal plume signature in the marine basin sediments above the suevitic deposits in the ~200 km Sudbury impact crater is characterized by elevated Zn, Cu, V, Cd, Ag, and Ni and extends over at least 25 km^2 within the post-impact marine shales (Rogers et al. 1995; Ames et al. 2002a). Characterization of the trace element signature of the basal Tertiary sequence above the Chicxulub impactites may identify post-impact hydrothermal precipitants from a crater floor vent system discharging metal-rich fluids into the Tertiary marine basin.

This paper documents the mineralogical and chemical effects of secondary alteration of the fragmental impactites, identifies a least-altered melt composition, and characterizes the mineralization in the basal Tertiary sequence of the Yaxcopoil-1 (Yax-1) drill core located within the Chicxulub crater.

GEOLOGIC SETTING OF THE YAX-1 DRILL HOLE

The Yax-1 drill hole is located on the Hacienda Yaxcopoil, 40 km southwest of Merida, Mexico at 20.740 °N

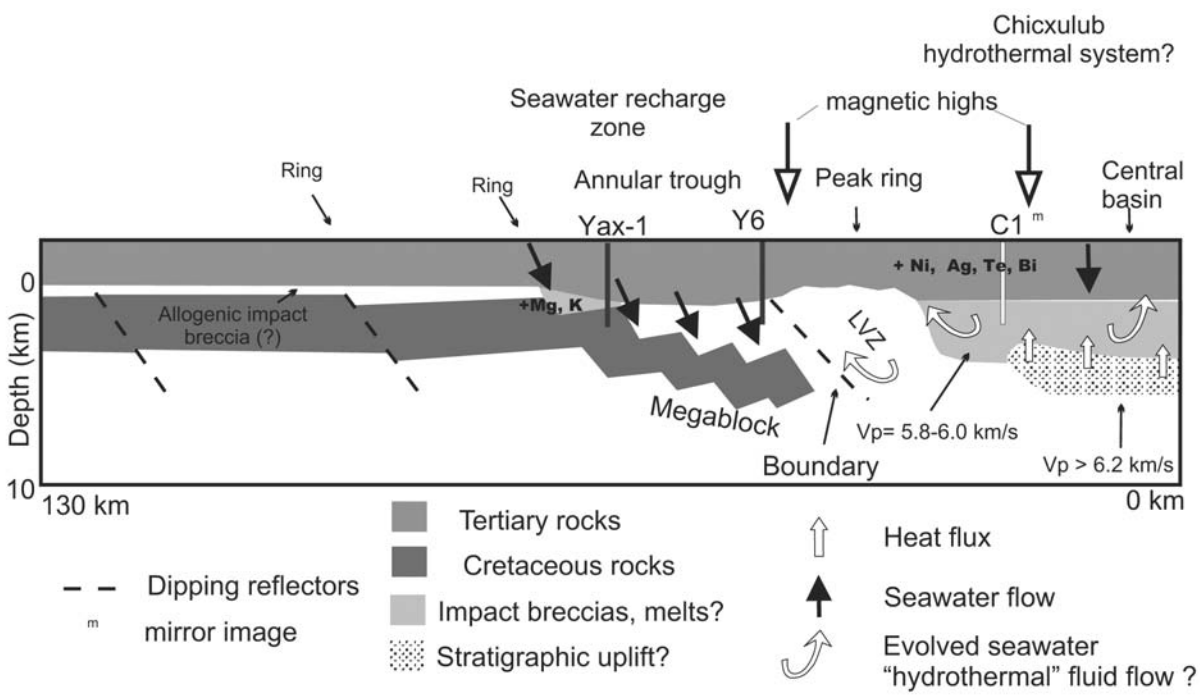

Fig. 1. Conceptual diagram displaying post-impact fluid flow on a cartoon of the Chicxulub crater. Ring faults and down-faulted mega block zones provide high-permeability pathways for seawater recharge in the annular trough environment, Yax-1 site location. Discharge/upflow zones are proposed in the central basin. The location of C-1 is shown in mirror image as it occurs on the opposite side of the central uplift from Yax-1. (compiled from Vermeesch and Morgan [2004] and Pilkington and Hildebrand [2000]).

89.718 °W. The drill hole was sited to continuously core the post-impact Tertiary sequence, the impact units, and the down faulted Cretaceous sedimentary rocks. The Yaxcopoil-1 drill hole intersected a faulted area in the outer annular trough (Dressler et al. 2003), ~68 km southwest of the center of the crater (Fig. 1). Data from Yax-1 may help determine whether faults in this area serve as a recharge zone where cold seawater penetrates into the impacted crust or as a focused discharge zone for the expulsion of evolved seawater or hydrothermal fluids (Fig. 1). The stratigraphic nomenclature used in this paper follows that of Dressler and others (2003), with units 1–6 comprising the impactite sequence intersected at 794.63 to 894.94 m (Fig. 2). The drill hole extended through the Tertiary sequence from 404 m to 794.63 m and underlying the impactites, the Cretaceous sequence was cored to 1511 m depth.

The suevite and melt rocks in the ~100 m-thick impactite sequence contain, on average, 60–95% altered blocky glass, now largely altered to clay minerals. The impact breccias and melt rocks cored include an ~14 m-thick, upper reworked suevite unit, a variety of 10–20 m-thick suevitic units, and an in situ brecciated melt showing hydroclastic fragmentation (~860–885 m, unit 5) (Fig. 2). Faults that form during the modification stage of impact cratering may provide high-permeability pathways that channel down-welling seawater and up-welling hydrothermal fluids. The highly permeable impactite sequence in Yax-1 may also channel fluid flow laterally and vertically.

The basal Tertiary rocks overlying the impactites at 794.63 m consist of a hemipelagic sequence of mid Eocene to lower-most Paleocene anoxic limestones, confirming that the crater filled with seawater soon after impact. The presence of reworked and redeposited suevite at the top of the impactite sequence also suggests a rapid influx of seawater after impact. The presence of this permeable substrate in a seawater-charged impact environment is conducive to sub-seafloor

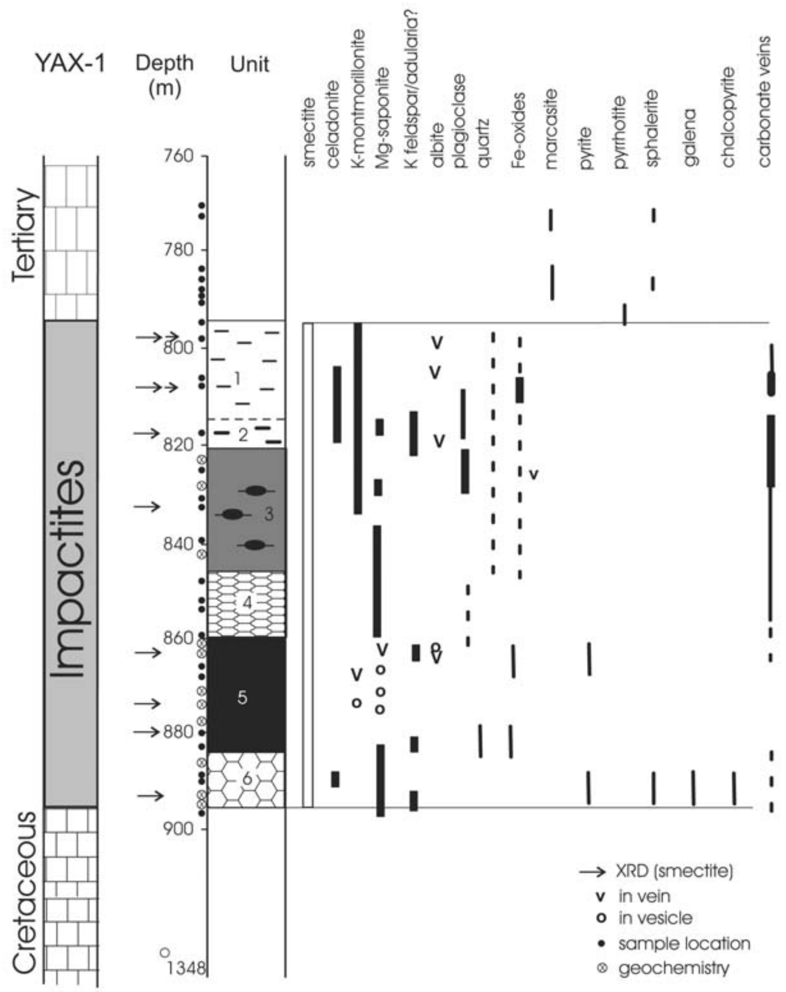

Fig. 2. Stratigraphic and alteration mineralogy section through the impact sequence and lower Tertiary carbonates in the Yax-1 drill hole. Unit 1 = redeposited suevite, unit 2 = suevite, unit 3 = melt-rich suevite, unit 4 = heterogeneous suevite, unit 5 = monomict melt breccia, unit 6 = variegated polymict melt breccia (Dressler et al. 2003). Sample locations are shown for petrography, geochemistry, and X-ray diffraction analyses.

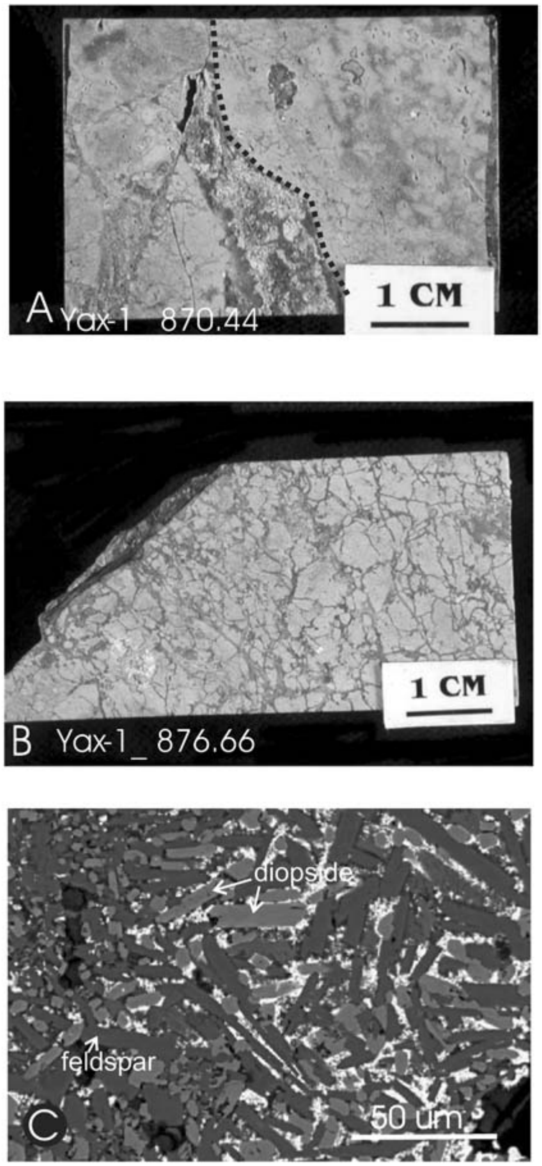

Fig. 3. Least-altered Yax-1 silicate melt: a) autobrecciated silicate melt, unit 5, Yax-1_870.44. Subsample for geochemistry to right of dashed line, dark green clay matrix for X-ray diffraction; b) hydroclastic fragmentation of silicate melt, Yax-1_876.66; c) SEM photograph of least altered silicate melt, Yax-1_867.57, unit 5. Dark grey laths = alkali feldspar, medium grey stubby laths = diopside, white = Fe-oxide.

fluid circulation and the formation of hydrothermal mineral deposits.

METHODOLOGY

Alteration mineral assemblages and mineral chemistry were documented from 25 polished thin sections made from the impactite sequence (Fig. 2). Eight additional samples at and above the suevite/Tertiary boundary at 794.2 m were studied, and the mineral chemistry was obtained for sulfide phases in the lowermost Tertiary strata (Fig. 2). The clay mineralogy of four fine whole rock (bulk) materials and six clay-size separates was determined by X-ray powder diffraction analysis (XRD) for samples extending from 798.06 m to 891.92 m within the suevite sequence (Fig. 2). Smear mounts were made by pipetting 40 mg suspensions (in water) of the clay-size separates onto glass slides and air-dried overnight to produce oriented mounts. X-ray patterns were recorded on a Bruker D8 Advance Powder Diffractometer equipped with a graphite monochromator. The Co Kα radiation was set at 40 kV and 40 mA. The samples were also X-rayed following saturation with ethylene glycol and heat treatment (550 ºC).

Microprobe analyses were obtained from a four-spectrometer wavelength dispersive CAMECA Camebax at Carleton University, Ottawa. Silicates, carbonates, and hydroxides were analyzed with 15 kV and 15 to 20 nA. Counting times were 10 sec for major elements and 20 sec for minor and trace elements including F and Cl. Clay minerals, carbonates, and hydroxides were analyzed with a strongly defocused beam (raster). The mineral chemistry of clay minerals and sulfide are in Tables 3 and 4. The standards used were: wollastonite for Si and Ca, spinel for Al, andradite for Fe, forsterite for Mg, albite for Na, orthoclase for K, MnTi for Mn and Ti, chromite for Cr, tugtupite for Cl, and LiF for F.

The geochemistry of the silicate melt component was determined for 16 samples of the impactites and one melt dyke cutting the underlying Cretaceous rocks (Fig. 2). Analyses were carried out by the Analytical Geochemistry Subdivision of the Geological Survey of Canada, Natural Resources Canada (Tables 1 and 2). The methods used include major element determinations by wavelength dispersive XRF, trace element determinations by inductively coupled-plasma emission (ICP-ES), and mass spectroscopy (ICP-MS). H_2O, C, and S were determined by infrared absorption, F and Cl by ion chromatography, and CO_2 by titration. Precision and accuracy were better than 5 percent and 2 sigma relative standard deviation (RSD), with measurements made relative to in-house reference material, duplicate samples, and international standards. During subsampling of the melt, care was taken to avoid veins, visible lithic fragments, fractures, and carbonate impurities.

PROTOLITH COMPOSITIONS OF LEAST-ALTERED MELT

Mineralogy and Mineral Chemistry

The least-altered silicate melt from Yax-1 was identified in unit 5, an in situ-brecciated melt approximately 24 m-thick (Fig. 2). Fine, 5–20 µm diopside microlites and coarser, <50 µm feldspar laths, commonly trachytic, are set in a subordinate matrix of finer magnetite, K-feldspar, quartz, and apatite (Fig. 3). The composition of the clinopyroxene in the

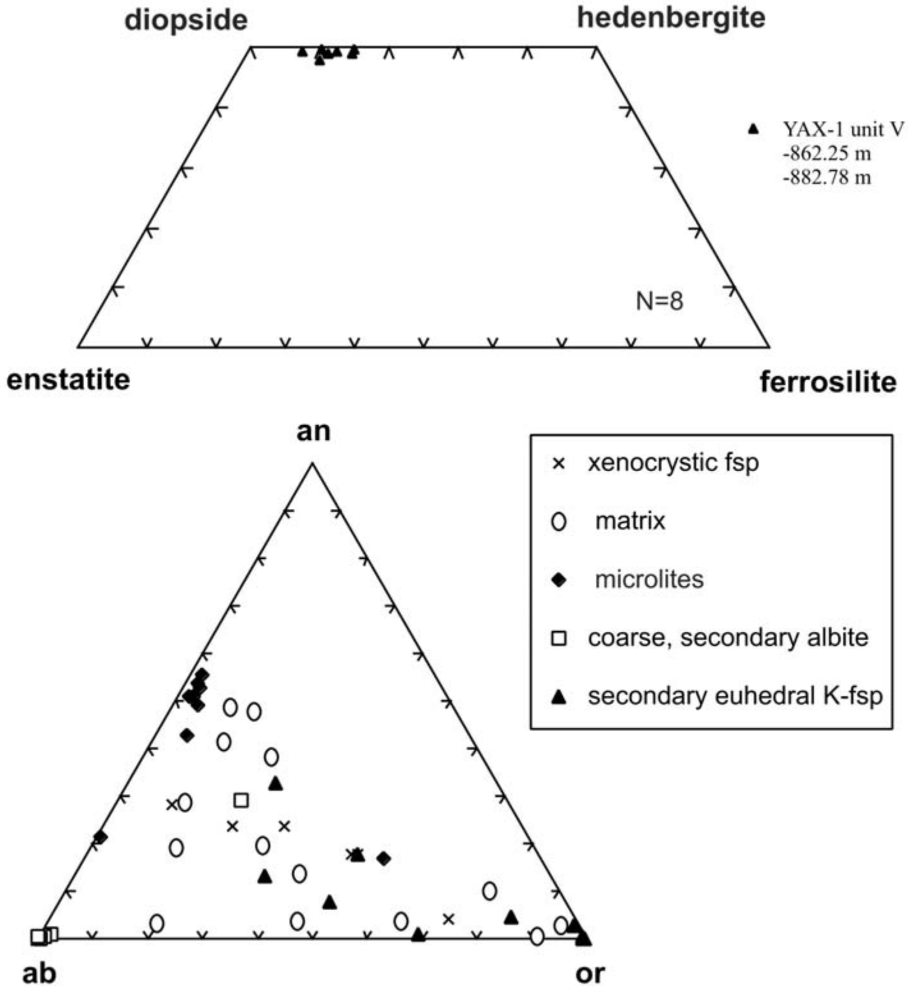

Fig. 4. Mineral chemical diagrams: a) pyroxene quadrilateral showing compositions of pyroxene in least-altered silicate melt, Yax-1; b) feldspar compositions from the impactites, Yax-1.

Yax-1 drill hole (Fig. 4a) is intermediate between diopside and hedenbergite (salite) with Mg numbers between 70–79. These are similar to that documented in the interpreted impact melt sheet samples C1-N10, Y6-N17, and N19 (Kring and Boynton 1992; Schuraytz et al. 1994). Feldspar microlites in the least-altered melt are dominantly plagioclase (Ab 37–47) set in a fine matrix of ternary feldspar intergrown with iron-oxides (Fig. 4b).

Geochemistry

The least-altered mineralogy of unit 5, in contrast to the clay-rich, clinopyroxene-poor mineralogy of altered silicate melt in other units, is used to characterize a primary silicate melt composition in the Yax-1 impactite sequence. Melt fragments were carefully selected to avoid alteration veinlets (Fig. 3). In terms of major element compositions, unit 5 is classified as a calc-alkaline basaltic andesite with 53.4–56 wt% SiO_2, ~6.93 wt% avg. MgO, and 15.9 wt% avg. Al_2O_3 (volatile-free; Figs. 5 and 6, Table 1). Ratios of relatively immobile elements TiO_2, Al_2O_3, and Zr in Y-6 and Yax-1 are similar, while C-1 contains higher Zr (155 ppm; Schuraytz et al. 1994). The higher MgO content of Yax-1 is accompanied by a decrease in SiO_2, likely showing that Mg metasomatism has also affected unit 5 composition possibly present as fine vesicles filled with smectite. The CO_2 content of the samples was used, in addition to petrography, to detect those samples contaminated by late carbonate that impregnated the matrix (Table 1). Silicate melt compositions normalized to average upper continental crust show a flat pattern which reflects the strong crustal signature of the impact melt in Yax-1 (Fig. 7).

ALTERATION OF THE IMPACTITE

Mineralogy and Mineral Chemistry

The most prominent alteration minerals impart a strong coloration to the impactite sequence with a predominance of bright green celadonite and brown to reddish-brown iron

Table 1. Geochemistry of silicate melt, Yax-1.

Sample	Yax-1 827.89	Yax-1 842.24	Yax-1 862.25	Yax-1 865.23	Yax-1 870.44	Yax-1 873	Yax-1 873.18	Yax-1 876.66	Yax-1 885.7	Yax-1 891.92A	Yax-1 891.99	Yax-1 893.33C	Yax-1 894.91
Depth	827.89	842.24	862.25	865.23	870.44	873	873.18	874.17	885.7	891.92A	891.99	893.33C	894.91
Descrip.	Silicate melt	Fgrd suevite-bright green glass	Fluidal breccia	Fluidal breccia	Fluidal breccia	Melt rock	Green monomict melt breccia	Fluidal breccia silicate melt	Bleached silicate melt	Silicate melt	Bleached melt rock	Silicate melt	Silicate melt (adj. to carb melt)
Unit	3	3	5	5	5	5	5	5	6	6	6	6	6
SiO_2	51.7	49.4	52.7	53.1	52.4	52.3	50.2	51.9	56.5	54.8	55.9	55.7	54.2
TiO_2	0.58	0.45	0.55	0.52	0.52	0.52	0.5	0.52	0.46	0.47	0.36	0.65	0.43
Al_2O_3	15.7	12.1	15	15.2	15.9	14.1	13.8	16	15.5	15.1	15.6	17	14.5
Fe_2O_{3T}	6.1	4.2	6.3	6.7	6.2	5.8	5.8	6.3	3.73	5.6	5.7	2.24	5.5
Fe_2O_3	5.21	3.31	4.63	5.14	4.64	3.57	3.35	4.85	–	4.82	5.03	2.02	4.72
FeO	0.8	0.8	1.5	1.4	1.4	2	2.2	1.3	–	0.7	0.6	0.2	0.7
MnO	0.01	0.01	0.02	0.02	0.03	0.06	0.08	0.02	0.06	0	0	0.03	0.01
MgO	5.57	8.07	7.48	6.93	6.29	6.11	5.86	6.69	0.31	5.74	5.09	0.56	5.91
CaO	4.99	7.98	6.54	6.5	8.42	10.71	12.79	7.57	8.38	4.18	4.57	8.12	5.78
Na_2O	2.9	2.3	3.1	3.4	3.6	3.4	3.3	3.5	3.6	3.4	3.5	3.41	3.3
K_2O	2.82	3.66	2.62	2.32	1.61	1.96	1.41	1.82	4.91	4.84	4.99	6.47	4.31
H_2O_T	6.8	6.9	4.7	4.6	3.9	2.7	2.6	4.6	–	3.7	3.1	0.6	3.6
CO_{2T}	0.9	4.7	0.1	0.1	0.1	1	2.9	0.7	4.7	0.7	1.3	4.2	1.9
P_2O_5	0.03	0.11	0.05	0.14	0.16	0.14	0.13	0.15	0.15	0.1	0.1	0.21	0.09
S_{total}	0.01	0.02	0.02	0.01	0.02	0.01	0.01	0.01	0.04	0.03	0.02	0.03	0.03
Ag	–0.1	–0.1	–0.1	–0.1	–0.1	–0.1	–0.1	–0.1	0.1	–0.1	–0.1	–0.1	–0.1
Ba	130	210	180	130	220	290	300	160	665	730	670	564	700
Be	1.5	0.9	1.4	1.3	1.3	1.1	1.1	1.4	0.9	1.1	1	1.4	1
Bi	–0.2	–0.2	–0.2	–0.2	–0.2	–0.2	–0.2	–0.2	0.2	0.3	0.3	0.3	0.3
Cd	–0.2	–0.2	–0.2	–0.2	–0.2	–0.2	–0.2	–0.2	–0.2	–0.2	–0.2	–0.2	–0.2
Co	8	13	13	12	14	15	14	12	–5	7	5	–5	7
Cr	74	47	62	64	67	58	59	63	41	46	40	70	41
Cs	1.6	0.63	1.3	1.1	0.81	0.54	0.51	0.94	0.31	0.68	0.63	0.22	0.64
Cu	–10	39	–10	16	22	10	14	–10	37	–10	–10	15	10
Ga	15	12	15	15	16	15	15	16	13	14	13	17	13
Hf	3.8	3.1	3.5	3.6	3.7	3.1	3.1	3.6	3.2	3.2	3.2	3.7	3.1
In	–0.05	–0.05	–0.05	–0.05	–0.05	0.06	0.05	–0.05	–0.05	–0.05	–0.05	–0.05	–0.05
Mo	–0.2	–0.2	–0.2	–0.2	–0.2	0.3	0.2	–0.2	0.4	–0.2	–0.2	0.3	–0.2
Nb	7.5	7	7.6	8.6	8.7	7.5	7.3	8.6	6.4	7	7.3	9.2	7.7
Ni	22	28	31	30	30	33	29	28	–10	20	16	–10	21
Pb	5	8	24	5	4	3	3	6	10	6	5	6	8
Rb	60	46	48	45	37	26	25	37	32	35	34	84	30
Sb	0.4	–0.2	0.3	0.3	0.2	0.2	0.7	–0.2	0.5	0.2	–0.2	0.6	0.4
Sc	19	16	19	19	20	19	19	19	3.4	11	10	12	14
Sn	1.2	1.2	2	1.1	1.1	2.7	1.8	1.1	2.4	1.6	1.8	2.9	2.1
Sr	431	425	484	479	538	534	505	531	496	554	596	446	545
Ta	0.55	0.42	0.5	0.53	0.53	0.47	0.46	0.54	0.64	0.55	0.57	0.56	0.52
Te	–0.2	–0.2	–0.2	–0.2	–0.2	–0.2	–0.2	–0.2	–0.2	–0.2	–0.2	–0.2	–0.2
Th	9.4	5.8	8.5	8.4	8.7	7.3	7.6	9.2	14	12	11	9	11
Tl	–0.02	0.02	–0.02	–0.02	–0.02	–0.02	–0.02	–0.02	0.02	–0.02	–0.02	0.09	–0.02
U	0.78	1.2	0.52	0.89	0.92	0.75	0.74	0.87	9.2	2	1.8	2.9	1.7
V	24	73	37	40	60	87	84	50	49	56	56	65	50

Table 1. Geochemistry of silicate melt, Yax-1. *Continued.*

Sample	Yax-1 827.89	Yax-1 842.24	Yax-1 862.25	Yax-1 865.23	Yax-1 870.44	Yax-1 873	Yax-1 873.18	Yax-1 876.66	Yax-1 885.7	Yax-1 891.92A	Yax-1 891.99	Yax-1 893.33C	Yax-1 894.91
Depth	827.89	842.24	862.25	865.23	870.44	873	873.18	874.17	885.7	891.92A	891.99	893.33C	894.91
Descrip.	Silicate melt	Fgrd suevite-bright green glass	Fluidal breccia	Fluidal breccia	Fluidal breccia	Melt rock	Green monomict melt breccia	Fluidal breccia silicate melt	Bleached silicate melt	Silicate melt	Bleached melt rock	Silicate melt	Silicate melt (adj. to carb melt)
Unit	3	3	5	5	5	5	5	5	6	6	6	6	6
Zn	51	65	60	40	43	48	48	44	32	31	29	32	35
Zr	122	115	122	128	132	111	111	135	90	108	112	154	111
Ce	12	39	25	29	37	67	45	60	32	23	25	55	23
Dy	1.6	3.4	1.6	4.4	4.4	3.4	2.8	3.4	1.7	1.4	1.6	4.3	1.4
Er	0.92	1.8	0.95	2.4	2.4	2	1.5	1.8	0.88	0.64	0.76	2.4	0.64
Eu	0.43	0.9	0.48	1.2	1.2	1	0.86	1	0.56	0.46	0.52	1.2	0.46
Gd	1.6	3.6	1.7	4.7	4.7	3.7	3.1	3.6	2.1	1.7	1.8	4.6	1.7
Ho	0.33	0.67	0.34	0.89	0.89	0.71	0.57	0.68	0.33	0.25	0.31	0.91	0.26
La	7.2	19	8.6	22	23	24	18	23	19	10	11	29	11
Lu	0.16	0.29	0.19	0.37	0.36	0.34	0.28	0.27	0.13	0.09	0.11	0.33	0.1
Nd	7.5	18	8.4	23	23	22	18	21	14	10	11	25	9.9
Pr	1.9	4.7	2.2	5.7	5.9	5.8	4.7	5.7	4	2.7	2.9	6.4	2.7
Sm	1.7	3.7	1.9	5	4.6	4.3	3.4	4.1	2.6	1.9	2.3	5	2
Tb	0.26	0.57	0.27	0.73	0.71	0.59	0.48	0.59	0.3	0.24	0.28	0.74	0.25
Tm	0.15	0.28	0.16	0.37	0.39	0.31	0.25	0.28	0.13	0.1	0.11	0.37	0.1
Y	8.8	21	8.8	25	26	21	17	19	10	7.2	8.4	27	7.6
Yb	1.1	1.8	1.2	2.4	2.4	2.1	1.7	1.8	0.84	0.58	0.75	2.3	0.61
Total	98.1	99.9	99.1	99.5	99.1	98.7	99.3	99.8	98.5	98.8	100.3	99.4	99.6

Table 2. Geochemistry of carbonate melt within impactite sequence and melt dyke within a Cretaceous block, Yax-1.

	Yax-1	Yax-1	Yax-1	Yax-1_
Sample	823.3	891.92B	893.33A	1348
Depth (m)	823.3	891.92B	893.33A	1348
Descrip.	Matrix	Melt	Melt	Melt dyke
Unit	3	6	6	
SiO_2	38.40	6.20	1.80	23.30
TiO_2	0.29	0.09	–0.02	0.51
Al_2O_3	10.00	1.40	0.30	10.30
Fe_2O_{3T}	4.30	1.10	0.16	4.70
Fe_2O_3	3.63	0.99	–	–
FeO	0.6	0.1	–	–
MnO	0.02	0.28	0.24	0.00
MgO	5.88	1.94	3.15	12.80
CaO	18.10	48.44	47.80	16.24
Na_2O	1.80	0.20	0.08	0.50
K_2O	2.23	0.30	0.20	3.70
H_2O_T	7.1	1.0	–	–
CO_{2T}	13.0	39.1	43.9	24.8
P_2O_5	0.05	0.01	–0.01	0.02
S_{total}	0.03	0.04	0.07	1.71
Ag	0.2	–0.1	–0.1	–0.1
Ba	210	82	799	150
Be	0.7	–0.5	–0.5	1.7
Bi	–0.2	–0.2	–0.2	0.3
Cd	–0.2	–0.2	–0.2	–0.2
Co	8	–5	–5	6
Cr	33	–10	–10	26
Cs	1.00	0.24	0.02	3.80
Cu	–10	–10	17	–10
Ga	11.00	2.10	0.90	12.00
Hf	2.10	0.35	0.06	3.80
In	–0.05	–0.05	–0.05	0.07
Mo	–0.2	–0.2	0.3	5.1
Nb	5.40	1.50	0.20	9.40
Ni	24	–10	–10	16
Pb	3	–1	1	11
Rb	38.00	7.90	1.50	–100.00
Sb	5.3	–0.2	0.3	0.7
Sc	11.0	3.9	1.9	12.0
Sn	0.5	–0.5	2.2	1.5
Sr	483	235	244	109
Ta	0.31	0.06	–0.05	0.59
Te	–0.2	–0.2	–0.2	–0.2
Th	4.40	0.94	0.12	9.10
Tl	0.02	–0.02	–0.02	1.20
U	1.00	0.73	0.51	3.60
V	30	12	6	25
Zn	56	19	19	37
Zr	84.0	16.0	2.0	143.0
Ce	46.0	12.0	20.0	27.0
Dy	2.40	1.10	1.30	3.40
Er	1.30	0.75	0.75	1.90
Eu	0.72	0.19	0.30	0.78
Gd	2.70	0.85	1.20	3.10
Ho	0.50	0.26	0.27	0.65
La	16.0	7.3	8.9	13.0
Lu	0.25	0.18	0.14	0.35
Nd	15.0	4.5	6.8	16.0
Pr	4.10	1.30	1.90	3.90
Sm	3.10	0.86	1.30	3.50
Tb	0.43	0.16	0.21	0.52
Tm	0.23	0.15	0.12	0.33
Y	13.00	8.10	9.10	19.00
Yb	1.60	1.10	0.85	2.20
Total	101.2	100.1	97.8	98.6

Table 2. Geochemistry of carbonate melt within impactite sequence and melt dyke within a Cretaceous block, Yax-1.

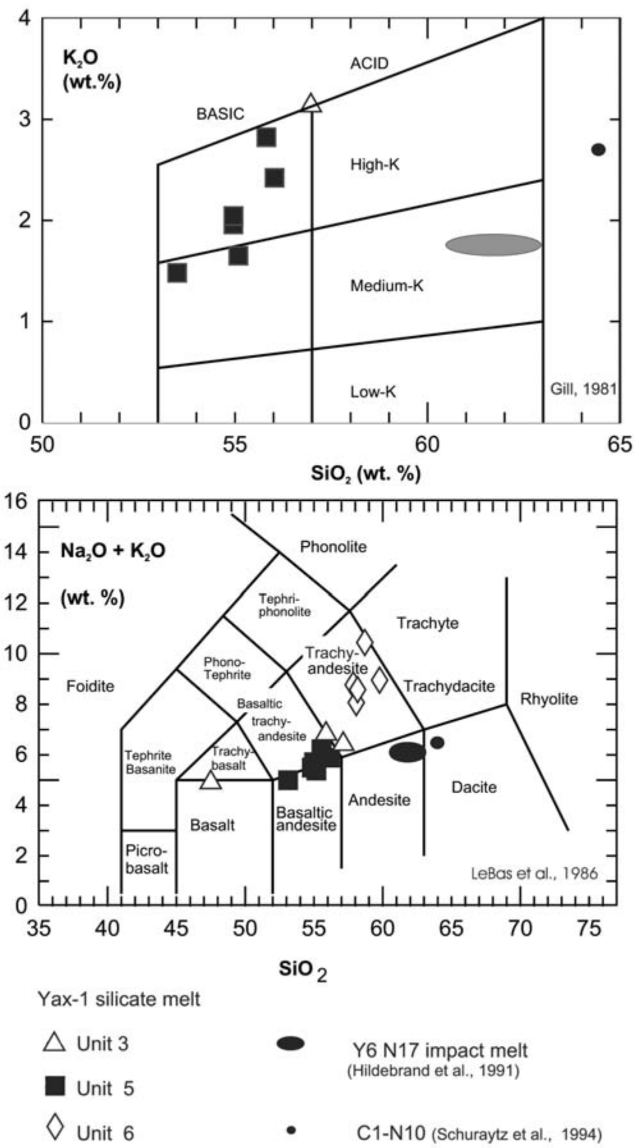

Fig. 5. Major element plots of the Yaxcopoil-1 suevitic melt rocks showing (a) the andesitic composition (volatile-free) of Yax-1 silicate melt after Gill (1981) and (b) total alkalis versus silica plots of LeBas et al. (1986).

oxide/goethite staining of the core (Fig. 8). Also present are varying amounts of Mg-saponite, K-montmorillonite, chalcedony, K-feldspar, magnetite, calcite, dolomite, and albite (Fig. 2). The details of the mineralogy and occurrence of the secondary Fe-oxides are documented in an accompanying paper (Pilkington et al. 2004).

Clay minerals in Yax-1 were characterized to determine possible mineral zonation, interstratification, and/or the possibility of fine-grained discrete phases. The clay minerals were identified by X-ray diffraction as pure smectite in 10 samples collected through the impactite sequence (Fig. 2). Celadonite, Mg-saponite, and K-montmorillonite identified

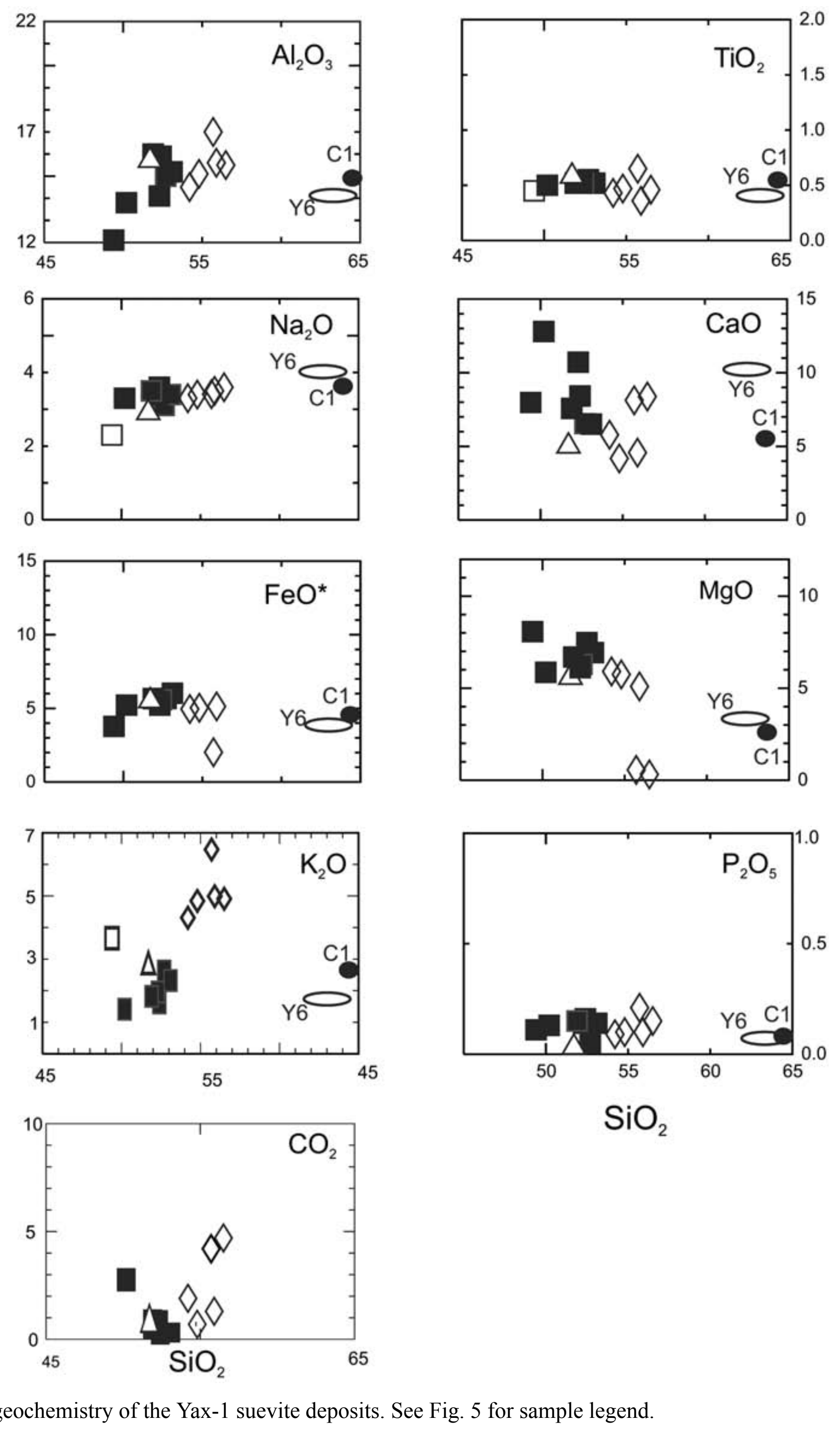

Fig. 6. Major element geochemistry of the Yax-1 suevite deposits. See Fig. 5 for sample legend.

Table 3. Clay mineral chemistry.[a]

Unit I						
Yax-1	806.41	807.99	807.99	807.99	807.99	807.99
Mineral	Mont.	Mont.	Mont.	Celadonite	Mont.	Mont.
Texture	Lining void	Matrix	Alt. glass	Lining amygd.	Lining amygd.	Amygd. rim
SiO_2	54.65	52.19	57.58	53.89	55.63	54.45
TiO_2	0.59	0.18	0.22	0.00	0.02	0.33
Al_2O_3	14.41	12.47	17.93	7.88	11.57	13.84
Cr_2O_3	0.00	0.01	0.00	0.01	0.00	0.02
FeO	7.80	13.35	2.56	18.19	5.42	9.40
MnO	0.06	0.01	0.02	0.04	0.06	0.00
NiO	0.02	0.06	0.00	0.03	0.06	0.06
MgO	5.92	7.88	5.84	5.79	9.96	5.54
CaO	1.30	0.65	0.87	0.49	0.11	0.84
BaO	0.00	0.00	0.00	0.04	0.00	0.00
Na_2O	0.28	1.13	2.64	0.82	0.41	1.78
K_2O	4.48	5.30	1.40	7.61	7.90	4.04
F	0.13	0.36	0.86	0.69	0.59	0.63
Cl	0.08	0.08	0.04	0.07	0.03	0.08
Subtotal[b]	89.71	93.66	89.94	95.55	91.75	91.02
Si	3.855	3.691	3.866	3.874	3.879	3.830
Ti	0.031	0.010	0.011	0.000	0.001	0.018
Al	1.198	1.040	1.419	0.668	0.951	1.148
Cr	0.000	0.001	0.000	0.001	0.000	0.001
Fe	0.460	0.789	0.144	1.093	0.316	0.553
Mn	0.003	0.000	0.001	0.002	0.003	0.000
Ni	0.001	0.003	0.000	0.002	0.003	0.003
Mg	0.623	0.830	0.584	0.621	1.035	0.581
Ca	0.098	0.049	0.062	0.038	0.008	0.063
Ba	0.000	0.000	0.000	0.001	0.000	0.000
Na	0.038	0.155	0.344	0.114	0.055	0.243
K	0.403	0.479	0.120	0.698	0.703	0.363
Al(IV)	0.114	0.300	0.123	0.126	0.120	0.153
Al(VI)	1.084	0.740	1.295	0.541	0.831	0.995
Mg + Fe	1.087	1.623	0.729	1.718	1.358	1.137
Ca + K + Na	0.539	0.682	0.526	0.851	0.766	0.669

Unit II					
Yax-1	818.05	818.05	818.05	818.05	818.05
Mineral	Mont.	Mont.	Mont.	Saponite	Mont.
Texture	Alt. glass	Matrix	Void filling	Alt. glass	Void filling
SiO_2	49.82	54.42	51.94	45.40	50.27
TiO_2	0.27	0.60	0.45	0.03	0.40
Al_2O_3	12.84	15.17	13.40	5.53	11.58
Cr_2O_3	0.02	0.00	0.00	0.00	0.00
FeO	6.91	7.17	10.19	3.12	9.19
MnO	0.00	0.05	0.00	0.04	0.00
NiO	0.00	0.04	0.00	0.00	0.03
MgO	5.33	6.00	5.17	22.94	5.70
CaO	0.78	1.38	0.73	0.39	0.66
BaO	0.00	0.06	0.06	0.04	0.00
Na_2O	1.06	0.56	0.83	1.00	1.04
K_2O	3.16	3.50	5.70	0.29	4.83
F	0.20	0.26	0.12	0.47	0.07
Cl	0.12	0.05	0.11	0.03	0.10
Subtotal[b]	80.53	89.25	88.69	79.27	83.86

Table 3. Clay mineral chemistry.[a] *Continued.*

Unit II					
Yax-1	818.05	818.05	818.05	818.05	818.05
Mineral	Mont.	Mont.	Mont.	Saponite	Mont.
Texture	Alt. glass	Matrix	Void filling	Alt. glass	Void filling
Si	3.889	3.829	3.807	3.571	3.870
Ti	0.016	0.032	0.025	0.001	0.023
Al	1.182	1.258	1.157	0.512	1.051
Cr	0.001	0.000	0.000	0.000	0.000
Fe	0.451	0.422	0.624	0.205	0.592
Mn	0.000	0.003	0.000	0.003	0.000
Ni	0.000	0.002	0.000	0.000	0.002
Mg	0.621	0.629	0.565	2.691	0.654
Ca	0.066	0.104	0.057	0.033	0.055
Ba	0.000	0.002	0.002	0.001	0.000
Na	0.161	0.076	0.118	0.152	0.155
K	0.314	0.314	0.533	0.029	0.474
Al(IV)	0.096	0.139	0.169	0.427	0.107
Al(VI)	1.086	1.119	0.988	0.085	0.944
Mg + Fe	1.072	1.056	1.189	2.899	1.247
Ca + K + Na	0.541	0.495	0.710	0.215	0.684
Unit III					
Yax-1	831.02	831.02	831.02	831.02	831.02
Mineral	Saponite	Saponite	Saponite	Saponite	Mont.
Texture	Dark red	Amyg. fill	Amyg. rim	Amyg. fill	Matrix
SiO_2	48.89	42.05	43.93	42.82	47.19
TiO_2	0.01	0.01	0.01	0.00	1.26
Al_2O_3	9.27	5.55	7.34	5.55	10.97
Cr_2O_3	0.02	0.03	0.00	0.02	0.00
FeO	3.98	4.68	4.29	3.81	6.64
MnO	0.05	0.04	0.01	0.00	0.05
NiO	0.00	0.00	0.03	0.07	0.00
MgO	19.27	19.97	18.62	21.14	7.24
CaO	1.32	0.93	1.97	1.00	0.77
BaO	0.03	0.01	0.07	0.00	0.03
Na_2O	0.47	0.98	0.44	1.22	0.74
K_2O	1.22	0.09	0.54	0.16	3.65
F	0.54	0.31	0.44	0.62	0.28
Cl	0.04	0.06	0.04	0.04	0.08
Subtotal[b]	85.10	74.72	77.73	76.46	78.90
Si	3.588	3.550	3.556	3.524	3.803
Ti	0.001	0.000	0.001	0.000	0.076
Al	0.802	0.553	0.700	0.539	1.041
Cr	0.001	0.002	0.000	0.001	0.000
Fe	0.244	0.331	0.290	0.262	0.447
Mn	0.003	0.003	0.001	0.000	0.003
Ni	0.000	0.000	0.002	0.004	0.000
Mg	2.108	2.514	2.247	2.594	0.870
Ca	0.103	0.084	0.171	0.088	0.067
Ba	0.001	0.000	0.002	0.000	0.001
Na	0.066	0.160	0.069	0.195	0.116
K	0.114	0.010	0.055	0.017	0.375
Al(IV)	0.411	0.449	0.444	0.476	0.121
Al(VI)	0.391	0.103	0.256	0.063	0.920
Mg + Fe	2.356	2.847	2.540	2.861	1.320
Ca + K + Na	0.285	0.255	0.298	0.300	0.559

Table 3. Clay mineral chemistry.[a] *Continued.*

Unit IV					
Yax-1	852.07	852.07	852.07	852.07	852.07
Mineral	Saponite	Saponite	Celadonite	Saponite	Saponite
Texture	Vermiform	Alt. glass	Alt. glass	Amygdule fill	Amygdule fill
SiO_2	45.35	42.73	52.38	41.20	40.68
TiO_2	0.11	0.01	0.49	0.12	0.01
Al_2O_3	7.81	6.35	10.71	6.87	5.96
Cr_2O_3	0.01	0.04	0.00	0.00	0.03
FeO	7.26	6.73	18.05	6.70	3.17
MnO	0.00	0.00	0.00	0.00	0.00
NiO	0.04	0.00	0.00	0.01	0.01
MgO	17.43	19.79	4.81	13.03	18.58
CaO	1.83	1.35	0.60	1.30	1.23
BaO	0.00	0.01	0.02	0.00	0.00
Na_2O	0.89	1.15	0.22	0.42	0.98
K_2O	1.37	0.21	6.69	1.18	0.09
F	0.24	0.18	0.04	0.07	0.32
Cl	0.10	0.06	0.08	0.08	0.06
Subtotal[b]	82.45	78.61	94.11	70.96	71.13
Si	3.537	3.483	3.790	3.698	3.573
Ti	0.007	0.001	0.027	0.008	0.001
Al	0.718	0.610	0.914	0.726	0.616
Cr	0.000	0.003	0.000	0.000	0.002
Fe	0.474	0.459	1.092	0.503	0.233
Mn	0.000	0.000	0.000	0.000	0.000
Ni	0.003	0.000	0.000	0.000	0.001
Mg	2.026	2.404	0.519	1.744	2.432
Ca	0.153	0.118	0.046	0.125	0.116
Ba	0.000	0.000	0.001	0.000	0.000
Na	0.135	0.181	0.031	0.074	0.168
K	0.136	0.022	0.618	0.135	0.010
Al(IV)	0.456	0.516	0.184	0.294	0.426
Al(VI)	0.262	0.094	0.730	0.433	0.191
Mg + Fe	2.503	2.863	1.611	2.247	2.666
Ca + K + Na	0.424	0.322	0.695	0.334	0.294

Unit V								
Yax-1	862.25	862.25	862.25	862.25	862.25	862.25	862.25	862.25
Mineral	Mont.	Saponite	Mont.	Bladed saponite	Bladed saponite	Mont.	Saponite	Mont.
Texture	Matrix	Filling amygd.	Amygdule rim	Lining vein	Lining vein	Filling vein	Filling amygd.	Amygd. rim
SiO_2	46.29	36.87	47.56	37.27	44.56	40.45	38.74	44.93
TiO_2	0.39	0.00	0.37	0.04	0.00	0.03	0.01	0.20
Al_2O_3	11.05	5.26	11.61	4.94	5.89	14.38	5.08	11.25
Cr_2O_3	0.02	0.04	0.02	0.00	0.00	0.00	0.00	0.04
FeO	9.02	4.92	6.98	4.73	5.96	3.70	5.06	4.58
MnO	0.04	0.00	0.01	0.01	0.05	0.02	0.01	0.01
NiO	0.03	0.03	0.00	0.00	0.00	0.08	0.02	0.01
MgO	5.28	17.38	6.23	16.76	20.52	8.05	18.61	5.72
CaO	0.50	1.05	0.47	1.70	2.01	1.45	1.37	1.29
BaO	0.03	0.00	0.01	0.06	0.05	0.00	0.01	0.01
Na_2O	0.54	0.50	0.56	0.46	0.18	0.63	0.77	0.52
K_2O	5.23	0.34	4.51	0.10	0.05	3.05	0.10	4.45
F	0.20	0.15	0.11	0.58	0.29	0.43	0.55	0.50

Table 3. Clay mineral chemistry.[a] *Continued.*

Unit V								
Yax-1	862.25	862.25	862.25	862.25	862.25	862.25	862.25	862.25
Mineral	Mont.	Saponite	Mont.	Bladed saponite	Bladed saponite	Mont.	Saponite	Mont.
Texture	Matrix	Filling amygd.	Amygdule rim	Lining vein	Lining vein	Filling vein	Filling amygd.	Amygd. rim
Cl	0.44	0.43	0.41	0.40	0.18	0.21	0.18	0.35
Subtotal[b]	79.05	66.97	78.86	67.04	79.74	72.48	70.52	73.86
Si	3.810	3.499	3.842	3.528	3.544	3.512	3.495	3.844
Ti	0.024	0.000	0.022	0.002	0.000	0.002	0.001	0.013
Al	1.072	0.588	1.105	0.551	0.552	1.472	0.540	1.134
Cr	0.001	0.003	0.001	0.000	0.000	0.000	0.000	0.003
Fe	0.621	0.391	0.472	0.374	0.396	0.269	0.382	0.328
Mn	0.003	0.000	0.001	0.001	0.003	0.001	0.001	0.000
Ni	0.002	0.002	0.000	0.000	0.000	0.006	0.002	0.000
Mg	0.648	2.459	0.750	2.365	2.433	1.042	2.502	0.730
Ca	0.044	0.106	0.041	0.173	0.172	0.135	0.133	0.118
Ba	0.001	0.000	0.000	0.002	0.002	0.000	0.000	0.000
Na	0.086	0.093	0.088	0.084	0.028	0.106	0.135	0.086
K	0.549	0.041	0.465	0.012	0.005	0.338	0.011	0.486
Al(IV)	0.167	0.501	0.135	0.470	0.456	0.486	0.504	0.143
Al(VI)	0.906	0.086	0.970	0.081	0.096	0.986	0.036	0.991
Mg + Fe	1.273	2.852	1.222	2.740	2.833	1.318	2.887	1.059
Ca + K + Na	0.680	0.240	0.594	0.270	0.206	0.579	0.279	0.691
Pt.	**20**	**21**	**22**	**49**	**50**	**54**	**55**	**56**
Unit VI								
Yax-1	882.78	882.78	882.78	889.63	889.63	889.63	889.63	889.63
Mineral	Mont.	Saponite	Saponite	Celadonite	Saponite	Saponite	Celadonite	Saponite
Texture	Surr. qtz	Flaky clay	Flaky clay	Green		Amygdule	Green	
SiO_2	39.21	38.59	35.69	51.75	52.12	45.24	52.80	41.97
TiO_2	0.32	0.03	0.00	0.15	0.04	0.06	0.12	0.00
Al_2O_3	7.93	5.66	4.56	9.07	7.72	5.26	8.59	5.23
Cr_2O_3	0.03	0.00	0.02	0.00	0.01	0.00	0.03	0.00
FeO	12.29	3.99	3.15	21.70	5.49	3.95	21.81	4.09
MnO	0.03	0.00	0.00	0.10	0.02	0.04	0.03	0.03
NiO	0.00	0.04	0.01	0.05	0.01	0.01	0.03	0.04
MgO	3.70	19.43	17.05	4.25	18.92	21.34	4.49	20.33
CaO	0.83	1.42	1.41	1.04	0.40	1.91	0.64	1.62
BaO	0.00	0.00	0.04	0.03	0.02	0.00	0.04	0.00
Na_2O	0.40	0.69	0.93	0.48	1.20	0.33	0.22	0.39
K_2O	5.15	0.14	0.16	7.03	3.43	0.30	7.68	0.18
F	0.34	0.19	0.42	0.05	0.47	0.40	0.07	0.47
Cl	0.09	0.07	0.09	0.11	0.02	0.06	0.03	0.05
Subtotal[b]	70.33	70.26	63.52	95.79	89.87	78.88	96.57	74.40
Si	3.782	3.472	3.541	3.778	3.691	3.598	3.822	3.550
Ti	0.023	0.002	0.000	0.008	0.002	0.004	0.007	0.000
Al	0.902	0.600	0.533	0.780	0.644	0.493	0.733	0.522
Cr	0.003	0.000	0.001	0.000	0.001	0.000	0.002	0.000
Fe	0.991	0.300	0.261	1.325	0.325	0.263	1.320	0.290
Mn	0.003	0.000	0.000	0.006	0.001	0.003	0.002	0.002
Ni	0.000	0.003	0.001	0.003	0.001	0.000	0.001	0.003
Mg	0.532	2.606	2.523	0.463	1.997	2.530	0.485	2.564
Ca	0.085	0.137	0.150	0.082	0.030	0.163	0.049	0.147
Ba	0.000	0.000	0.002	0.001	0.000	0.000	0.001	0.000

Table 3. Clay mineral chemistry.[a] *Continued.*

Pt.	**20**	**21**	**22**	**49**	**50**	**54**	**55**	**56**
Unit VI								
Yax-1	882.78	882.78	882.78	889.63	889.63	889.63	889.63	889.63
Mineral	Mont.	Saponite	Saponite	Celadonite	Saponite	Saponite	Celadonite	Saponite
Texture	Surr. qtz	Flaky clay	Flaky clay	Green		Amygdule	Green	
Na	0.076	0.121	0.179	0.067	0.165	0.051	0.031	0.064
K	0.634	0.016	0.020	0.655	0.310	0.030	0.710	0.019
Al(IV)	0.195	0.526	0.459	0.214	0.308	0.398	0.171	0.450
Al(VI)	0.707	0.074	0.075	0.566	0.337	0.095	0.562	0.072
Mg + Fe	1.526	2.909	2.784	1.796	2.323	2.796	1.808	2.859
Ca + K + Na	0.795	0.273	0.350	0.804	0.506	0.244	0.791	0.230

[a]Mont = Montmorillonite: $(Na, Ca)_{0.3}(Al, Mg)_2Si_4O_{10}(OH)_2.nH_2O$; Saponite: $(Ca/2, Na)_{0.3}(Mg, Fe^{2+})_3(Si, Al)_4O_{10}(OH)_2.4H_2O$; montmorillonite is very fine-grained and grey or colorless lining amygdules, shards, and veins; saponite is coarser and bladed, forming thick, brownish linings around shards, amygdules, and veins; celadonite is greenish-brown.

[b]Subtotal not including H_2O; formula calculation based on 11 oxygens (water-free).

through mineral chemistry (Table 3, Fig. 9) typically replace clinopyroxene in melt fragments throughout the fragmental impactite sequence. They also line and fill, amygdales and veins and replace the matrix. Mg-rich saponite is brownish and fibrous, while the K-montmorillonite is generally clear, fine-grained, and concentrically zoned within amygdales. Compositions of the clays are intermediate between the two end members saponite and montmorillonite, with the Yax-1 montmorillonite containing some Mg and the saponite containing some Al_2O_3 (Table 3). Both minerals are elevated in potassium (Fig. 9). Characteristic bright green celadonite is abundant as a secondary phase in veins and amydales and fills open spaces throughout the impactite sequence. Veins of celadonite also crosscut the strongly magnetic mafic basement clasts that are found throughout the suevite in Yax-1 (889.63 m) (see Pilkington et al. 2004). Although not exclusive, Mg-saponite dominates the upper 40 m of the impactites, while K-montmorillonite is abundant in the lower ~60 m (Fig. 2).

Chlorite, which is optically and chemically distinctive from the saponite-montmorillonite-celadonite clay minerals, was not identified by mineral chemistry or petrographically in 25 thin sections nor by X-ray diffraction of 10 samples through the impactite sequence (Fig. 2). This is in contrast to a report by Zürcher and Kring (2003) based solely on mineral chemistry and petrography. Neither is there evidence of clay replacing chlorite or interstratified clay-chlorite minerals. Trace chlorite was identified in a small basement fragment of sericite-feldspar schist and, clearly, is not part of the alteration assemblage. Chlorite is chemically quite different from the composition of the prevalent Chicxulub clay minerals, with chlorite being much more Al- and Fe-rich and Si- and K-poor relative to the comparatively Si-, Mg-, and K-rich clays found in all of the rocks examined in Yax-1.

Chalcedony occurs within the upper reworked units (806.41, 807.99, and 818.05), with a light green, amorphous mineral with an intense blue fluorescence (Fig. 8d). These amorphous minerals line amygdales, some of which were infilled earlier with fine euhedral K-feldspar.

K-feldspar occurs as euhedral rhomb shaped crystals lining voids, occurring as replacement alteration haloes on veins commonly associated with Mg-saponite and fine magnetite in the matrix (Fig. 4b). K-feldspar-magnetite replacement haloes on veins are found near the upper and lower contacts of the in situ brecciated melt, unit 5 (861 to 885 m) (Fig. 2). Trace amounts of coarse end member albite formed later in veins, voids, and within porous melt fragments (Fig. 4b, 8b, and 8c).

Trace amounts of sulfide are present in the impactite sequence. Pyrite, chalcopyrite, low-iron sphalerite and rare galena were observed. (Co-Ni) pyrite is associated with chalcopyrite near the base of the impactite sequence (894.88). Fine, <50 μm grains are cored by sphalerite and rimmed with chalcopyrite dusted with very fine (<5 μm) galena.

The last mineral phase to form was secondary calcite. It replaces earlier dolomite in the impact breccia and pseudomorphs "glass" shards. Calcite locally forms the matrix to altered melt fragments and fills amygdales, some of which are already lined with K-feldspar or clay minerals and fractures (Fig. 8e). Earlier-formed dolomite rhombs in the secondary carbonate matrix of the impactite are overgrown by late calcite. Calcite also occurs in unit 1 (806.41) as spherical grains, possibly droplets and as fragments in silicate glass, which is presently altered to K-montmorillonite (Fig. 8f). Secondary calcite veining is most abundant in units 1 to 3 and least common in the in situ-brecciated silicate melt rock of unit 5.

Geochemistry

The geochemistry of altered melt in units 3 and 6 are compared with the least-altered andesitic composition of unit 5 in Yax-1 as well as melt compositions from Y-6 and C-1 (Figs. 5 and 6). The unit 6 suevite has significantly elevated

Table 4. Sulfide mineral chemistry from the basal Tertiary rocks, Yax-1.[a]

Depth	770.43	770.43	770.43	770.43	770.43	772.46	772.46	783.65	783.65	783.65	785.64	785.64	785.64	787.85	787.85
Mineral	Sphalerite	Marcasite	Marcasite	Marcasite	Marcasite	Marcasite	Marcasite	Marcasite	Marcasite	Marcasite	Marcasite	Marcasite	Marcasite	Sphalerite	Marcasite
Descrip.	Tiny crystal in py	Bladed	Massive	Fine gr. spongy	Edge	Pseudo-cubic xx	Pseudo-cubic xx	Lace-like intergrowth w. carbonate		Fortress shaped	Coarse, euh. X	Coarse, euh. X, core	Coarse, euh. X, rim	Tiny incl. in py	Blocky, euh.
V	0.04	0.00	0.00	0.00	0.00	0.00	0.02	0.01	0.02	0.01	0.02	0.01	0.02	0.01	0.02
Mn	0.02	0.00	0.02	0.05	0.00	0.00	0.01	0.01	0.02	0.00	0.01	0.01	0.00	0.03	0.02
Fe	3.09	46.95	47.28	47.48	47.77	47.57	47.68	47.16	47.47	47.84	47.10	47.31	47.05	2.55	46.56
Ni	0.02	0.01	0.01	0.01	0.02	0.00	0.01	0.03	0.02	0.01	0.12	0.00	0.02	0.01	0.01
Cu	1.06	0.00	0.02	0.01	0.03	0.00	0.05	0.05	0.00	0.02	0.06	0.02	0.02	0.35	0.01
Zn	65.45	0.00	0.02	0.02	0.06	0.01	0.01	0.02	0.00	0.03	0.04	0.00	0.00	67.34	0.00
Cd	1.39	0.02	0.00	0.05	0.05	0.07	0.00	0.00	0.04	0.04	0.01	0.02	0.04	0.22	0.00
In	0.00	0.03	0.01	0.00	0.00	0.01	0.00	0.00	0.02	0.01	0.00	0.01	0.03	0.00	0.00
Ga	1.08	0.03	0.00	0.00	0.00	0.00	0.00	0.00	0.00	0.01	0.00	0.00	0.03	0.47	0.02
Sn	0.22	0.03	0.01	0.00	0.01	0.00	0.00	0.00	0.01	0.00	0.01	0.01	0.00	0.23	0.00
Ag	0.03	0.07	0.00	0.06	0.02	0.00	0.00	0.00	0.01	0.01	0.06	0.06	0.02	0.00	0.00
Au	0.00	0.04	0.09	0.00	0.07	0.11	0.00	0.00	0.03	0.00	0.00	0.05	0.00	0.00	0.13
Hg	0.00	0.08	0.06	0.00	0.01	0.08	0.10	0.01	0.07	0.02	0.10	0.01	0.00	0.01	0.07
Bi	0.00	0.01	0.00	0.00	0.09	0.03	0.02	0.06	0.00	0.00	0.05	0.00	0.02	0.00	0.00
Te	0.00	0.00	0.03	0.00	0.05	0.00	0.05	0.00	0.00	0.00	0.02	0.00	0.00	0.01	0.00
Sb	0.00	0.02	0.00	0.01	0.00	0.00	0.00	0.00	0.00	0.03	0.00	0.01	0.00	0.01	0.02
As	0.01	0.00	0.00	0.01	0.00	0.00	0.00	0.02	0.00	0.00	0.01	0.03	0.02	0.06	0.00
Se	0.00	0.00	0.00	0.00	0.00	0.01	0.02	0.04	0.00	0.02	0.00	0.02	0.00	0.01	0.00
S	31.97	53.39	53.74	53.36	53.49	53.62	53.29	53.44	53.89	53.72	53.91	54.01	53.67	32.65	54.08
Total	104.37	100.67	101.27	101.04	101.67	101.50	101.26	100.84	101.63	101.77	101.50	101.56	100.93	103.94	100.94
V	0.000	0.000	0.000	0.000	0.000	0.000	0.000	0.000	0.000	0.000	0.000	0.000	0.000	0.000	0.000
Mn	0.000	0.000	0.000	0.000	0.000	0.000	0.000	0.000	0.000	0.000	0.000	0.000	0.000	0.000	0.000
Fe	0.026	0.335	0.335	0.338	0.338	0.337	0.339	0.336	0.335	0.338	0.333	0.334	0.334	0.022	0.330
Ni	0.000	0.000	0.000	0.000	0.000	0.000	0.000	0.000	0.000	0.000	0.001	0.000	0.000	0.000	0.000
Cu	0.008	0.000	0.000	0.000	0.000	0.000	0.000	0.000	0.000	0.000	0.000	0.000	0.000	0.003	0.000
Zn	0.476	0.000	0.000	0.000	0.000	0.000	0.000	0.000	0.000	0.000	0.000	0.000	0.000	0.488	0.000
Cd	0.006	0.000	0.000	0.000	0.000	0.000	0.000	0.000	0.000	0.000	0.000	0.000	0.000	0.001	0.000
In	0.000	0.000	0.000	0.000	0.000	0.000	0.000	0.000	0.000	0.000	0.000	0.000	0.000	0.000	0.000
Ga	0.007	0.000	0.000	0.000	0.000	0.000	0.000	0.000	0.000	0.000	0.000	0.000	0.000	0.003	0.000
Sn	0.001	0.000	0.000	0.000	0.000	0.000	0.000	0.000	0.000	0.000	0.000	0.000	0.000	0.001	0.000
Ag	0.000	0.000	0.000	0.000	0.000	0.000	0.000	0.000	0.000	0.000	0.000	0.000	0.000	0.000	0.000
Au	0.000	0.000	0.000	0.000	0.000	0.000	0.000	0.000	0.000	0.000	0.000	0.000	0.000	0.000	0.000
Hg	0.000	0.000	0.000	0.000	0.000	0.000	0.000	0.000	0.000	0.000	0.000	0.000	0.000	0.000	0.000
Bi	0.000	0.000	0.000	0.000	0.000	0.000	0.000	0.000	0.000	0.000	0.000	0.000	0.000	0.000	0.000
Te	0.000	0.000	0.000	0.000	0.000	0.000	0.000	0.000	0.000	0.000	0.000	0.000	0.000	0.000	0.000
Sb	0.000	0.000	0.000	0.000	0.000	0.000	0.000	0.000	0.000	0.000	0.000	0.000	0.000	0.000	0.000
As	0.000	0.000	0.000	0.000	0.000	0.000	0.000	0.000	0.000	0.000	0.000	0.000	0.000	0.000	0.000
Se	0.000	0.000	0.000	0.000	0.000	0.000	0.000	0.000	0.000	0.000	0.000	0.000	0.000	0.000	0.000
S	0.474	0.664	0.664	0.661	0.660	0.662	0.660	0.663	0.663	0.661	0.665	0.665	0.665	0.482	0.669
Total	1.000	1.000	1.000	1.000	1.000	1.000	1.000	1.000	1.000	1.000	1.000	1.000	1.000	1.000	1.000

Table 4. Sulfide mineral chemistry from the basal Tertiary rocks, Yax-1.[a] *Continued.*

Depth	787.85	787.85	787.85	787.85	787.85	788.64	788.64	788.64	788.64	788.64	789.61	789.61	789.61	789.61	789.61
Mineral	Marcasite	Marcasite	Marcasite	Marcasite	Marcasite	Marcasite	Marcasite	Marcasite	Marcasite	Marcasite	Pyrrhotite	Pyrrhotite	Pyrrhotite	Pyrrhotite	Pyrrhotite
Descrip.	Blocky, core	Blocky, rim	Spongy core	Solid rim	Massive	Bladed	Bladed	Massive	Massive	Massive	Euhedral bladed	Bladed, rim	Bladed, core	Bladed	Bladed, rim
V	0.00	0.01	0.01	0.00	0.00	0.02	0.01	0.02	0.00	0.01	0.01	0.01	0.01	0.01	0.01
Mn	0.01	0.00	0.02	0.01	0.00	0.00	0.00	0.00	0.00	0.00	0.00	0.00	0.01	0.03	0.00
Fe	48.52	47.70	46.24	47.83	47.89	47.90	47.65	48.25	47.72	47.42	60.42	60.42	60.72	60.60	60.41
Ni	0.03	0.00	0.00	0.01	0.01	0.00	0.00	0.00	0.00	0.00	0.02	0.05	0.05	0.01	0.23
Cu	0.04	0.00	0.03	0.04	0.00	0.02	0.02	0.00	0.02	0.00	0.00	0.00	0.09	0.00	0.00
Zn	0.02	0.04	0.04	0.00	0.00	0.00	0.00	0.01	0.03	0.00	0.04	0.05	0.03	0.03	0.02
Cd	0.00	0.04	0.01	0.04	0.00	0.00	0.02	0.03	0.00	0.00	0.00	0.01	0.00	0.00	0.02
In	0.03	0.00	0.03	0.00	0.02	0.00	0.02	0.02	0.00	0.00	0.03	0.00	0.00	0.00	0.00
Ga	0.02	0.00	0.00	0.00	0.01	0.00	0.01	0.00	0.00	0.01	0.04	0.02	0.00	0.00	0.00
Sn	0.02	0.00	0.00	0.02	0.00	0.00	0.01	0.00	0.02	0.00	0.05	0.00	0.00	0.00	0.01
Ag	0.00	0.00	0.00	0.01	0.00	0.07	0.00	0.05	0.03	0.02	0.00	0.00	0.04	0.00	0.00
Au	0.01	0.09	0.00	0.00	0.00	0.00	0.00	0.05	0.01	0.04	0.00	0.00	0.12	0.00	0.00
Hg	0.06	0.00	0.03	0.00	0.00	0.00	0.00	0.00	0.00	0.12	0.00	0.00	0.04	0.12	0.02
Bi	0.04	0.00	0.01	0.06	0.03	0.00	0.04	0.00	0.00	0.00	0.01	0.00	0.00	0.00	0.00
Te	0.00	0.02	0.00	0.00	0.00	0.02	0.00	0.01	0.00	0.00	0.08	0.00	0.01	0.01	0.00
Sb	0.00	0.00	0.00	0.02	0.00	0.01	0.01	0.00	0.00	0.00	0.00	0.00	0.00	0.00	0.01
As	0.00	0.02	0.00	0.02	0.00	0.00	0.01	0.01	0.00	0.02	0.00	0.07	0.05	0.01	0.00
Se	0.00	0.00	0.03	0.00	0.02	0.00	0.00	0.00	0.00	0.00	0.00	0.00	0.00	0.00	0.00
S	54.60	54.79	52.62	54.55	54.53	54.46	54.47	54.43	54.42	54.03	39.67	40.16	40.44	39.58	40.08
Total	103.41	102.71	99.07	102.62	102.50	102.49	102.27	102.90	102.26	101.68	100.36	100.77	101.62	100.39	100.82
V	0.000	0.000	0.000	0.000	0.000	0.000	0.000	0.000	0.000	0.000	0.000	0.000	0.000	0.000	0.000
Mn	0.000	0.000	0.000	0.000	0.000	0.000	0.000	0.000	0.000	0.000	0.000	0.000	0.000	0.000	0.000
Fe	0.337	0.333	0.335	0.335	0.335	0.335	0.334	0.337	0.335	0.335	0.466	0.463	0.462	0.467	0.463
Ni	0.000	0.000	0.000	0.000	0.000	0.000	0.000	0.000	0.000	0.000	0.000	0.000	0.000	0.000	0.002
Cu	0.000	0.000	0.000	0.000	0.000	0.000	0.000	0.000	0.000	0.000	0.000	0.000	0.001	0.000	0.000
Zn	0.000	0.000	0.000	0.000	0.000	0.000	0.000	0.000	0.000	0.000	0.000	0.000	0.000	0.000	0.000
Cd	0.000	0.000	0.000	0.000	0.000	0.000	0.000	0.000	0.000	0.000	0.000	0.000	0.000	0.000	0.000
In	0.000	0.000	0.000	0.000	0.000	0.000	0.000	0.000	0.000	0.000	0.000	0.000	0.000	0.000	0.000
Ga	0.000	0.000	0.000	0.000	0.000	0.000	0.000	0.000	0.000	0.000	0.000	0.000	0.000	0.000	0.000
Sn	0.000	0.000	0.000	0.000	0.000	0.000	0.000	0.000	0.000	0.000	0.000	0.000	0.000	0.000	0.000
Ag	0.000	0.000	0.000	0.000	0.000	0.000	0.000	0.000	0.000	0.000	0.000	0.000	0.000	0.000	0.000
Au	0.000	0.000	0.000	0.000	0.000	0.000	0.000	0.000	0.000	0.000	0.000	0.000	0.000	0.000	0.000
Hg	0.000	0.000	0.000	0.000	0.000	0.000	0.000	0.000	0.000	0.000	0.000	0.000	0.000	0.000	0.000
Bi	0.000	0.000	0.000	0.000	0.000	0.000	0.000	0.000	0.000	0.000	0.000	0.000	0.000	0.000	0.000
Te	0.000	0.000	0.000	0.000	0.000	0.000	0.000	0.000	0.000	0.000	0.000	0.000	0.000	0.000	0.000
Sb	0.000	0.000	0.000	0.000	0.000	0.000	0.000	0.000	0.000	0.000	0.000	0.000	0.000	0.000	0.000
As	0.000	0.000	0.000	0.000	0.000	0.000	0.000	0.000	0.000	0.000	0.000	0.000	0.000	0.000	0.000
Se	0.000	0.000	0.000	0.000	0.000	0.000	0.000	0.000	0.000	0.000	0.000	0.000	0.000	0.000	0.000
S	0.661	0.666	0.664	0.665	0.665	0.664	0.665	0.662	0.665	0.665	0.533	0.536	0.536	0.532	0.535
Total	1.000	1.000	1.000	1.000	1.000	1.000	1.000	1.000	1.000	1.000	1.000	1.000	1.000	1.000	1.000

[a]Co and Pb were analyzed but not detected.

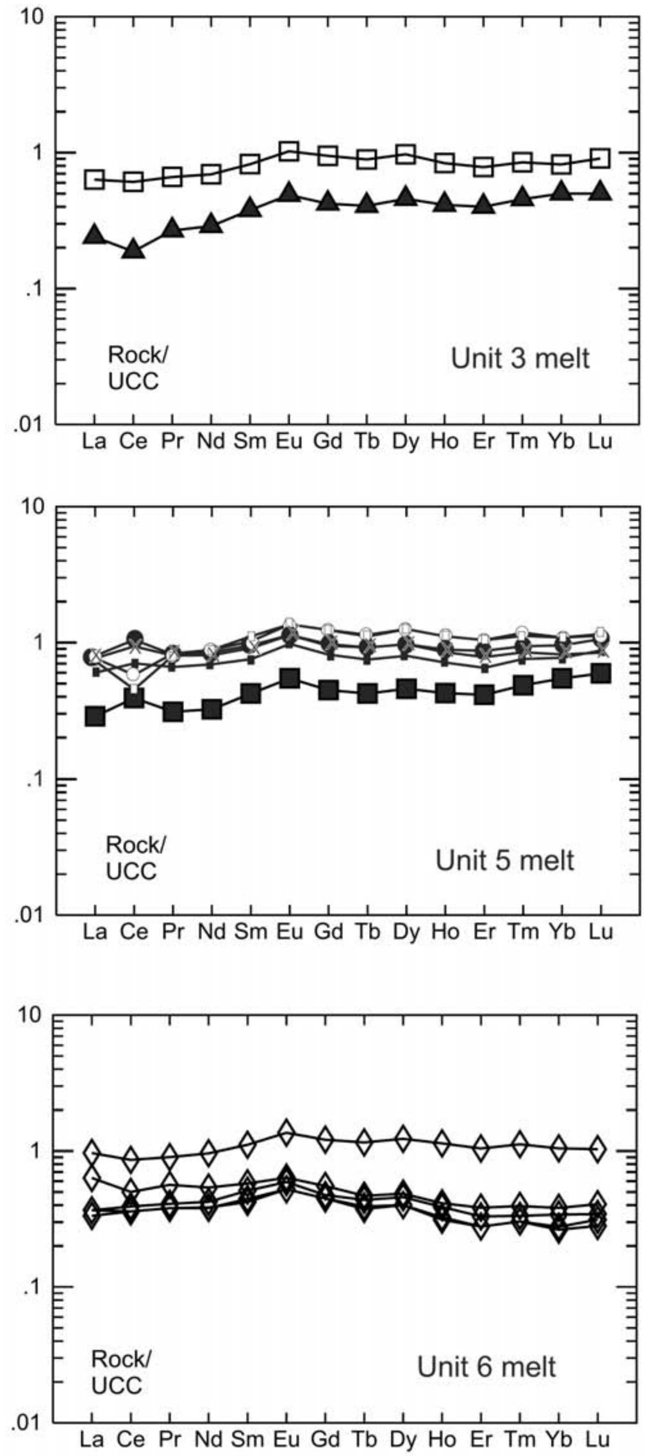

Fig. 7. Upper continental crust-normalized REE patterns for the silicate melt in the annular trough at Yax-1.

K_2O contents reaching up to 7 wt%, and some samples of unit 3 show only a minor addition of K_2O (Fig. 6). The suevite (unit 6) composition at the base of the sequence trends into the trachyandesite fields due to this addition of K_2O (Fig 5 and 6; Table 1). All of the suevite and melt samples in Yax-1 show elevated MgO relative to that in Y-6 and C-1 (Fig. 6).

MINERALIZATION IN THE LOWER TERTIARY SEQUENCE

Above the impactite sequence at 894.88 m are coarse 1–3 cm sulfide-smectite aggregates in the Tertiary limestone cover rocks (Fig. 10). They are composed of bladed to blocky pseudo-cubic marcasite with minor anhedral pyrrhotite, pyrite, and trace sphalerite. Strongly anisotropic, skeletal, sieve-textured marcasite is overgrown by blocky pseudo-cubic, euhedral marcasite in a calcite matrix (Fig. 11). In sample 789.61, the Fe-sulfide phase is pyrrhotite. Trace amounts of sphalerite occur within marcasite as fine <5 μm grains with elevated Ga and Cd. The mineral chemistry indicates elevated trace element values in Ag, Te, Au, Ni, and Bi, irrespective of the marcasite crystal habit (Table 4; Fig. 12).

DISCUSSION

The least-altered andesitic composition of the melt in Yax-1 differs significantly from melt compositions in Y-6 and C-1 which are located closer to the center of the crater (Figs. 1 and 6). Yax-1 melt composition shows elevated MgO, while the Y-6 and C-1 silicate melt has elevated SiO_2, which may reflect either dilution due to Mg metasomatism reflected by the ubiquitous smectite in Yax-1 or may reflect compositional heterogeneities in the impact melt (Fig. 6). Schuraytz and others (1994) also show variation in melt geochemistry from two holes (Y-6 and C-1) closer to the center of the crater, attributing differences to variations in local target rocks and depth of melting. Studies of the Y-6 core, also drilled in the annular trough ~20 km north of Yax-1, suggest that the silicate melt was not appreciably hydrothermally altered (Kring and Boynton 1992), but the chemistry indicates elevated SiO_2 and Na_2O relative to the composition of silicate melt in Yax-1.

In modern and ancient seafloor hydrothermal systems (Galley 1993; Alt 1995; Hannington et al. 1995), the addition of Mg and K (Mg-smectite and K-feldspar) from seawater sources occurs in relatively cool recharge zones (T = 0–150 °C). Metasomatic reactions between down-welling seawater and the volcanic pile occur at progressively higher temperatures with depth, producing stacked extensive semi-conformable alteration zones, the strike length of which is limited to strata overlying the heat source to the sub-seafloor convective system (Galley 1993). Zonation is characterized at shallow levels by Mg-K-enriched clay-zeolite metasomatic facies (50–140 °C), followed downward by Na-Mg enrichment at moderate temperatures (140–300 °C) reflected in chlorite-albite alteration ± mixed layered chlorite-smectite to chlorite and high temperature, Na-Ca-Fe-enriched greenschist-amphibolite metasomatic facies (>300 °C) at depths proximal

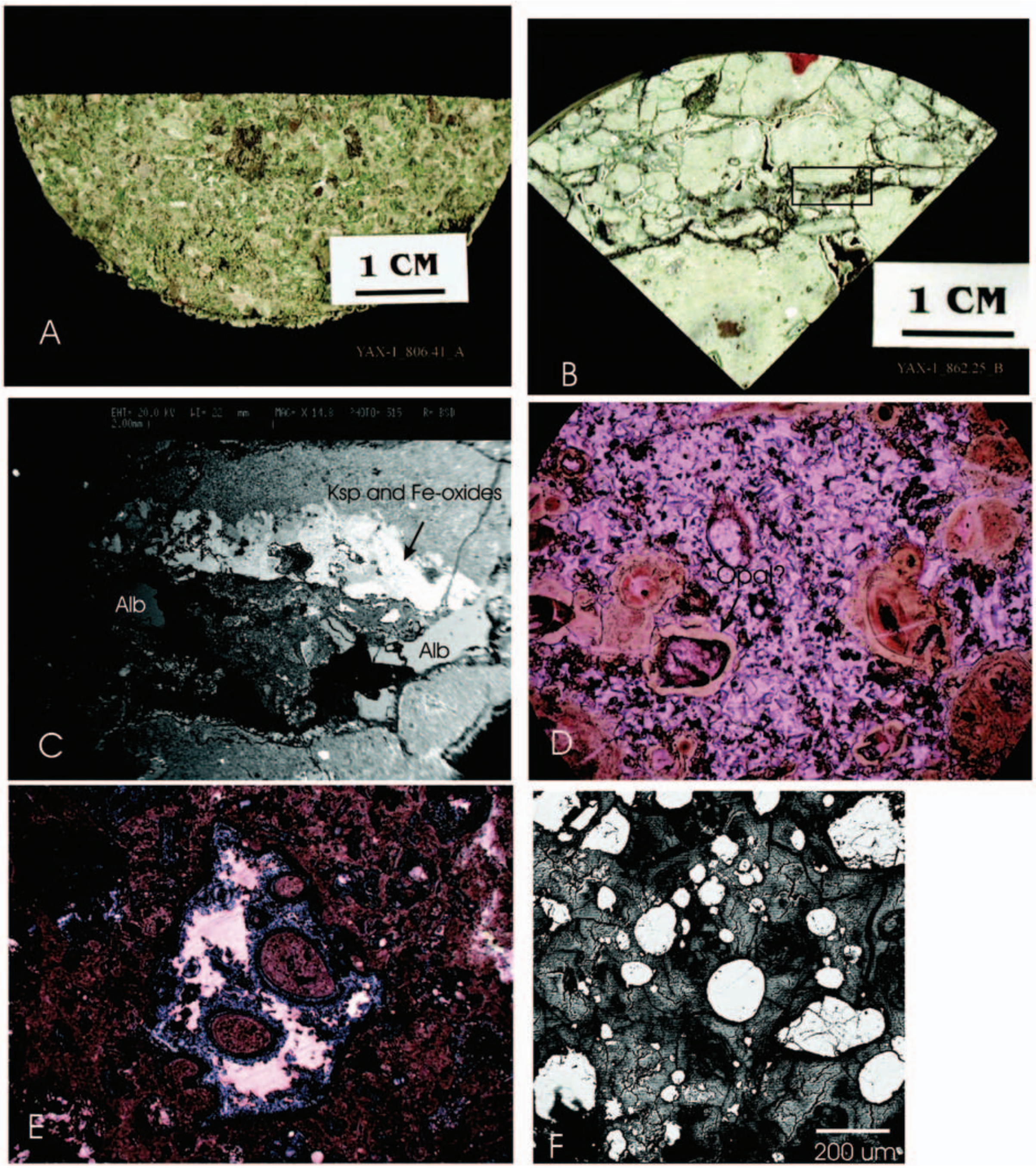

Fig. 8. Representative alteration types in the Yax-1 drill core, Chicxulub: a) bright green celadonite alteration of the reworked suevite, unit 1, 806.41m; b) dark brown K-feldspar, Fe-oxide veins near the top of unit 5, 862.25 m. The box shows the location of the SEM photo in (c); c) potassic alteration haloes on albite-Fe-oxide veins cutting unit 5, 862.25 m. Location of (b) shown in (c); d) green amorphous mineral (opal?) concentrically lining voids now filled with euhedral K-feldspar rhombs, 807.99 m, unit 1; e) vesicular shard replaced by coarse secondary calcite in a matrix of fine granular carbonate forming the matrix, 832.54 m; f) calcite fragments and droplets in altered silicate glass, K-montmorillonite, unit 1, 806.41 m.

to the heat source. The trend to lower greenschist facies minerals is reflected by the appearance of mixed layer chlorite-smectite, chlorite, actinolite replacing clinopyroxene, and albite partially replacing plagioclase, but these assemblages are not present in Yax-1. High temperature reaction zones generally contain the assemblage actinolite-hornblende-clinopyroxene and epidote. In the large Sudbury impact crater, regional, vertically stacked alteration zones occur with increasing depth and paleo-temperatures (up to 250–300 °C) in the impact crater fill sequence (Ames et al. 1998, 2002b).

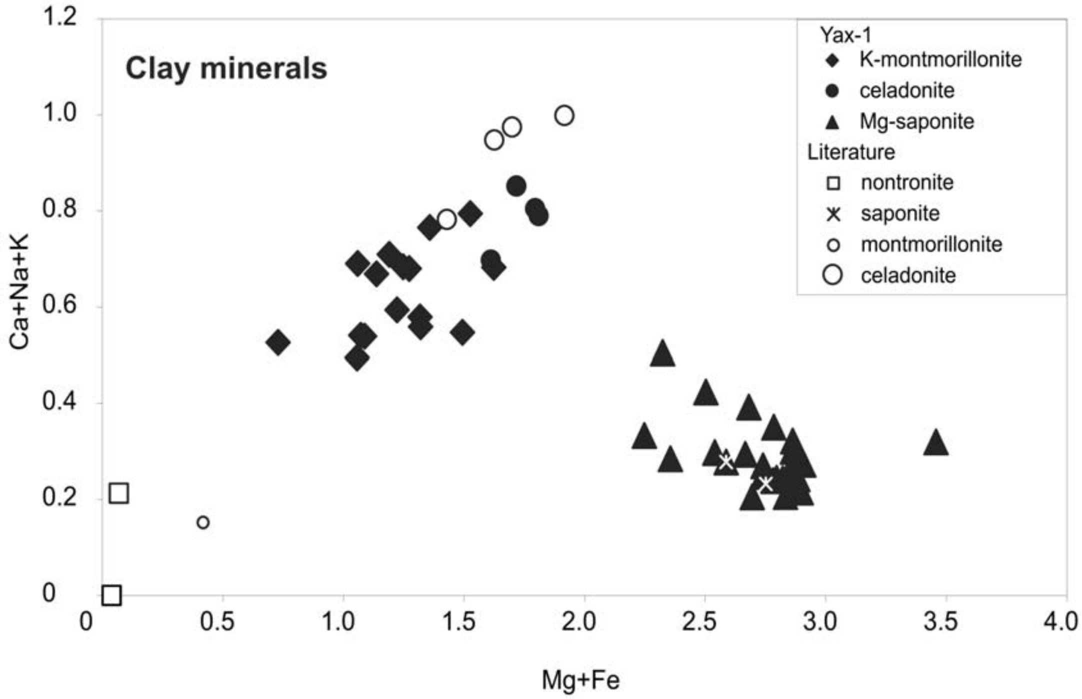

Fig. 9. Bivariate plot of the clay mineral compositions in Yax-1. The solid symbols are those from this study; the open symbols are for nontronite, saponite, and montmorillonite from Anthony et al. (1990); the celadonite compositions are from Pflumio (1991).

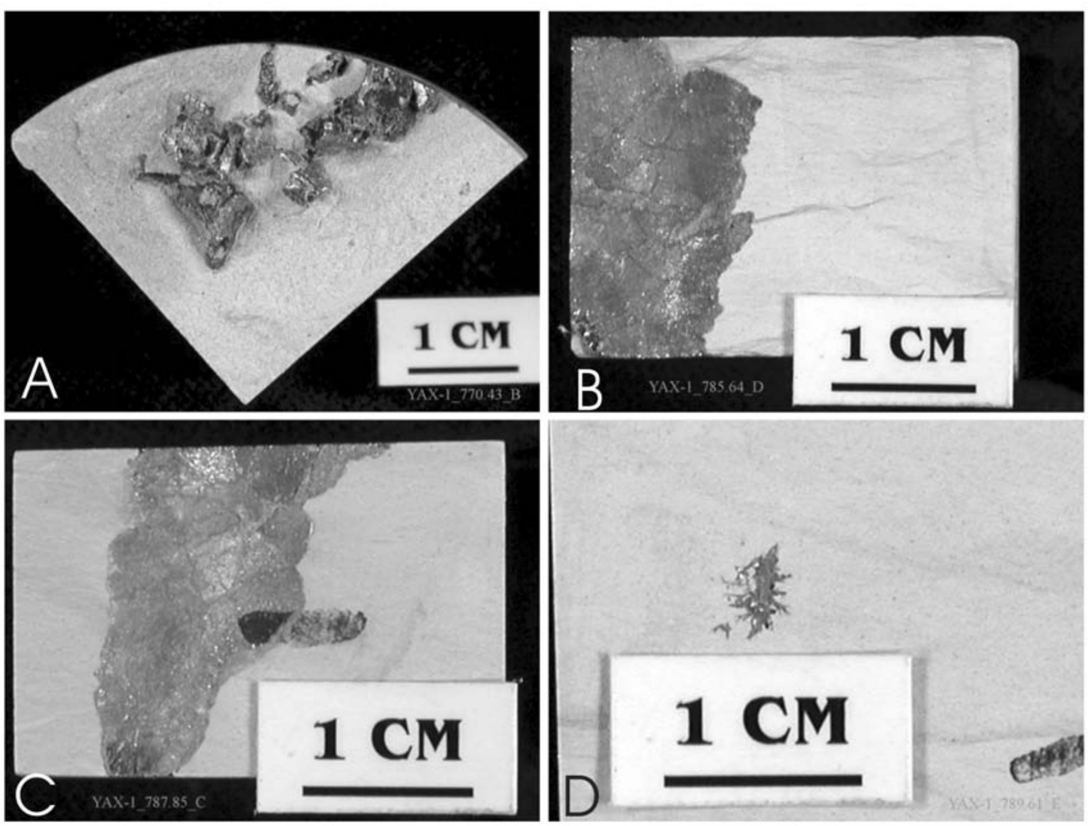

Fig. 10. Representative sulfide aggregates in the lower 25 m of the Tertiary sequence, (770.43–789.61 m) Chicxulub, Yax-1: a) euhedral marcasite crystals in Tertiary carbonates, 770.43 m; b) photomicrographs of massive marcasite rimmed with a clay-rich alteration halo, 785.64 m; c) 787.85 m; d) Bladed radiating pyrrhotite in Tertiary carbonate matrix, 789.61 m.

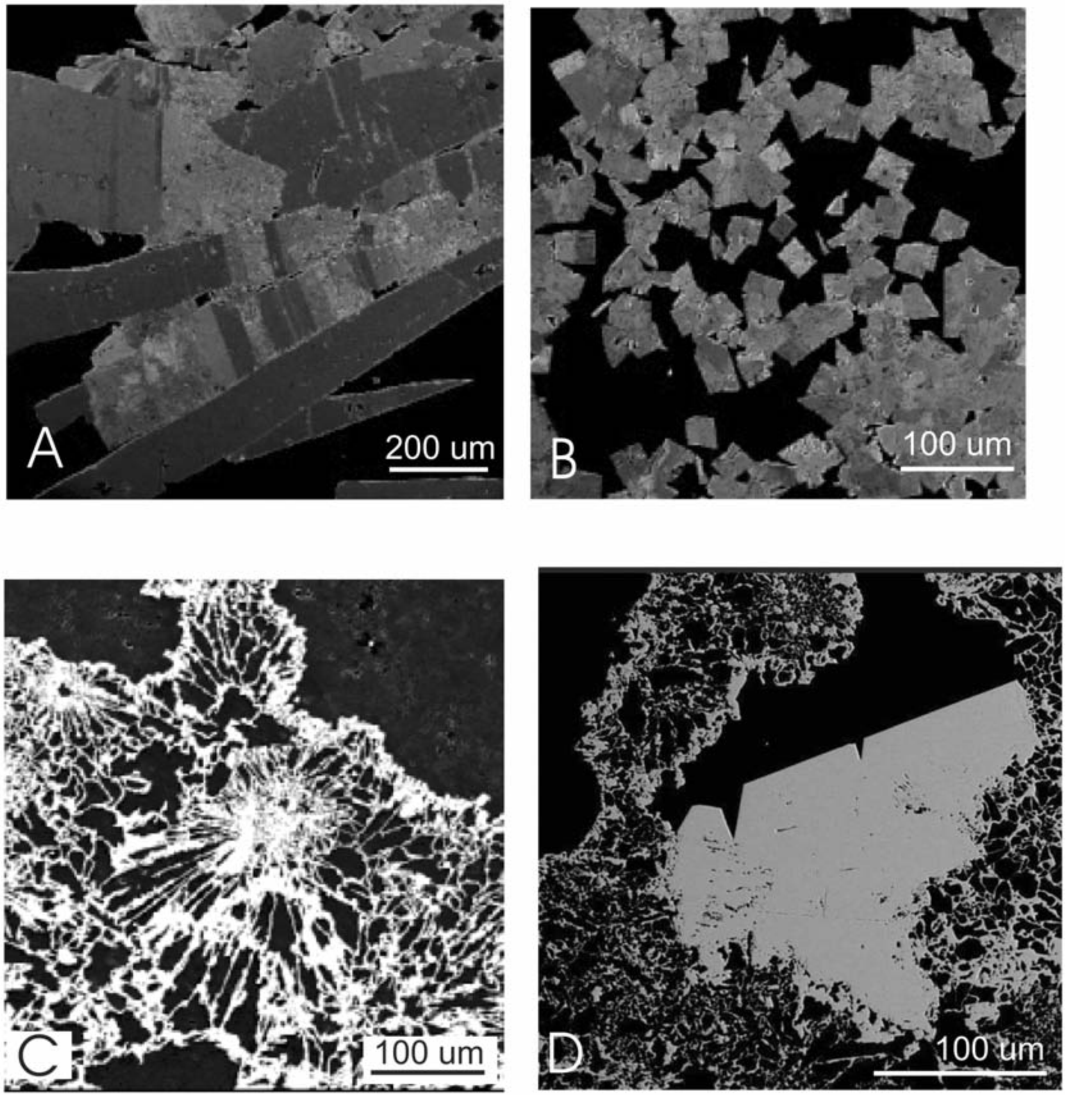

Fig. 11. Textural features of marcasite in the lower Tertiary carbonate sequence, Yax-1: a) optically strongly zoned heterogeneous bladed marcasite, 770.43 m; b) pseudocubic marcasite crystals, 772.48 m; c) early skeletal marcasite intergrown with carbonate (dark), 783.65 m; d) pseudocubic marcasite overgrowth on earlier skeletal marcasite, 783.65 m.

Alteration of the Yax-1 core characterized by Mg-saponite, K-montmorillonite, celadonite, Fe-oxides, and K-feldspar is typical of low-temperature (0–150 °C) seawater recharge zones. Alkali fixation from seawater resides in K-feldspar as well as the smectites filling fractures and vesicles in the rocks (Fig. 9). The mean FeO/FeO + MgO (wt%) content of saponite from Yax-1 is 0.21, similar to saponites affected by open, oxidizing alteration in the crust (0.3) in contrast to those saponites (~0.48) formed due to more restricted low temperature alteration (Alt 1995). Oxidizing conditions are also reflected by the abundance of Fe-oxides (Pilkington et al. 2004) and the paucity of Cu-Fe-Zn-Pb sulfide minerals within the Yax-1 impactites. Mg fixation in the Yax-1 impactites is evident by the dominant clay Mg-saponite, which, in the absence of mixed layered chlorite-smectite, indicates low temperatures of formation. Zeolite minerals and chlorite were not identified in the Yax-1 core, indicating that hydrothermal temperatures >150 °C were not attained at this site in the annular trough environment. Alteration of mafic glass results in quartz-saturated fluids (Berndt et al. 1989) that precipitated in vesicles and open spaces in the Yax-1 impactite. The secondary minerals Fe-oxides, celadonite, Mg-saponite, K-montmorillonite, K-feldspar formed during low temperature oxidation and fixation of alkalis and Mg due to cold seawater infiltration into the highly permeable impact sequence.

Crater Floor Hydrothermal Vents and Massive Sulfide Deposits?

The lack of significant hydrothermal alteration of the impactites in the Yax-1 core is consistent with the core's

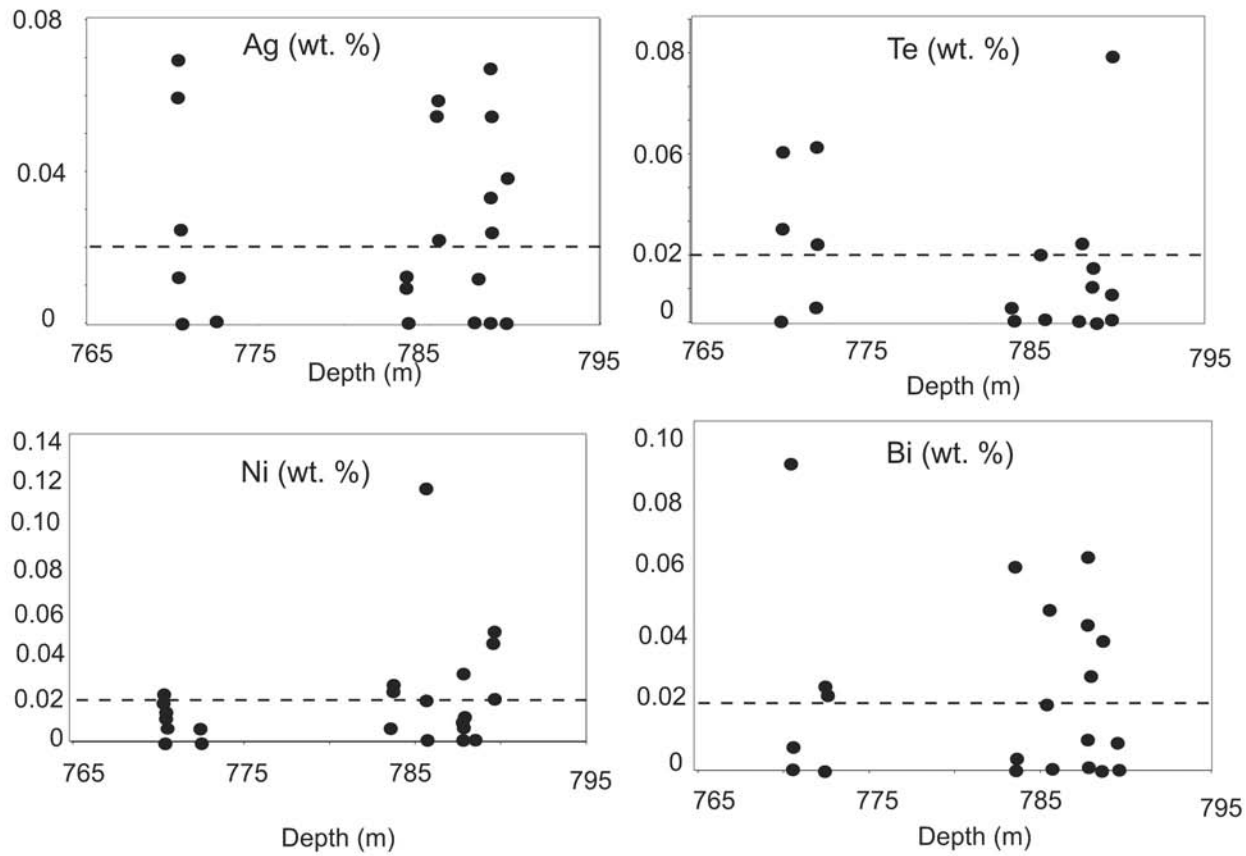

Fig. 12. Trace element compositions of marcasite with depth, Yax-1.

location outside of the concentric magnetic zones attributed to hydrothermal alteration by Pilkington and Hildebrand (2000). If a robust post-impact hydrothermal system developed in the Chicxulub crater-fill closer to the central basin, with its associated melt sheet and central uplift, hydrothermal vents may have developed on the crater floor as they did at Sudbury (e.g. Rousell 1984; Ames et al. 2000, 2002a). Indeed, trace element analyses from the Yax-1 core do indicate some hydrothermal discharge into the Tertiary basin at Chicxulub. Elevated Ag, Te, Ni, Au, and Bi in marcasite within the basal Tertiary carbonate rocks suggest hydrothermal enrichment from a mafic source. Magnetic mafic basement fragments in Yax-1 (Pilkington et al. 2004) and isotopic data from Y-6 and C-1 impact melts (Kettrup et al. 2000) support a significant mafic component to the basement and, consequently, to the impact melt that was generated. This has important implications for potential economic hydrothermal sulfide deposits in the Chicxulub crater. The robust paleo-hydrothermal system at the large Sudbury crater produced Zn-Pb-Cu-Ag-Au massive sulfide deposits and exhalites. The massive sulfide deposits indicate focused hydrothermal venting at 200–250 °C, while the exhalites that are in part carbonate-facies iron formation indicate lower temperature but extensive, diffuse low temperature venting over large areas (Ames et al. 1998, 2000, 2002a). The sulfide deposits of the Sudbury crater floor vent systems are a modest economic resource at 6.4 Mt (Ames et al 2002b), however the magmatic Ni-Cu and magmatic-hydrothermal Cu-PGE deposits that developed at the base of the Sudbury melt sheet comprise the largest mineral deposits in the world (e.g., Naldrett 2003).

CONCLUSIONS

The calc-alkalic basaltic andesite composition of the melt component in the Yax-1 impactites has been strongly affected by low temperature alkali-magnesium fixation and oxidation. We have demonstrated that the alteration mineral assemblages identified through petrography, X-ray diffraction, and mineral chemistry are the result of low temperature (<150 °C) seawater interaction with andesitic glass in the suevite contained in the outer annular trough at Chicxulub. This seawater recharge zone may be feeding a higher temperature impact-generated system closer to center of the crater as suggested by the hydrothermal plume trace element signature identified in the basal Tertiary sulfides reflecting hydrothermal venting into the Tertiary ocean.

Although hints of hydrothermal activity occur in the annular trough environment of the Chicxulub crater in the Tertiary system, only deep drilling closer to the center of the crater will provide conclusive evidence for a thick melt sheet and a post-impact hydrothermal system with potential economic resources.

Acknowledgments–This work was supported by the NASA Exobiology program (Grant NAG5–10744) and Natural Resources Canada. We would like to recognize the efforts of ICDP and UNAM for making the cores available and of Igor Bilot and Bradley Harvey at the Geological Survey of Canada for sample preparation and photography. Jeanne Percival is also acknowledged for clay mineral identification through X-ray diffraction. Reviews by Kalle Kirsimae, Horton Newsom, and Philippe Claeys have improved the manuscript. This is Geological Survey of Canada contribution 2003247.

Editorial Handling—Dr. Philippe Claeys

REFERENCES

Alt J. C. 1995. Subseafloor processes in mid-ocean ridge hydrothermal systems. In *Seafloor hydrothermal systems: Physical, chemical, biological, and geological interactions,* edited by Lupton J., Mullineaux L., and Zierenberg R. Geophysical Monograph 91. Washinton D.C.: American Geophysical Union. pp. 85–114.

Berndt M. E., Seal R. R., II, Shanks W. C., III, and Seyfried W. E. 1994. D/H fractionation during phase separation of seawater in subseafloor hydrothermal systems: Isobaric heating and adiabatic decompression (abstract). Proceedings, Goldschmidt Conference.

Ames D. E., Gibson H. L., and Watkinson D. H. 2000. Controls on major impact-induced hydrothermal system, Sudbury structure, Canada (abstract #1873). 31st Lunar and Planetary Science Conference. CD-ROM.

Ames D. E., Watkinson D. H., and Parrish R. R. 1998. Dating of a hydrothermal system induced by the 1850 Ma Sudbury impact event. *Geology* 26:447–450.

Ames D. E. 2002. Sudbury targeted geosciences initiative (TGI: 2000–2003): Overview and update. Summary of field work and other activites 2002. Ontario Geological Survey Open File Report 6100. pp. 17-1–17-10.

Ames D. E., Pope K. O., Jonasson I. R., and Hofmann B. 2002a. Chemical sediments associated with the impact-generated hydrothermal system, Vermilion formation, Sudbury structure. Geological Society of America Annual Meeting.

Ames D. E., Golightly J. P., Lightfoot P. C., and Gibson H. L. 2002b. Vitric compositions in the Onaping formation and their relationship to the Sudbury igneous complex, Sudbury structure. *Economic Geology* 97:1541–1562.

Anthony J. W., Bideaux R. A., Bladh K. W., and Nichols M. 1990. *Handbook of mineralogy, vol II: Silicates.* Tucson: Mineral Data Publishing.

Baker E. T., German C. R., and Elderfield H. 1995. Hydrothermal plumes over spreading-center axes: Global distributions and geological inferences. In *Seafloor hydrothermal systems: Physical, chemical, biological, and geological interactions,* edited by Lupton J., Mullineaux L., and Zierenberg R. Geophysical Monograph 91. Washington D.C.: American Geophysical Union. pp. 47–71.

Dressler B. O., Sharpton V. L., Morgan J., Buffler R., Moran D., Smit J., Stöffler D., and Urrutia J. 2003. Investigating a 65-Ma-old smoking gun: Deep drilling of the Chicxulub impact structure. *EOS Transactions* 84:125.

Farrow C. E. G. and Watkinson D. H. 1991. An evaluation of the role of fluids in Ni-Cu-PGE-bearing, mafic-ultramafic systems. *Geological Association of Canada Short Course Notes* 13:31–67.

Galley A. G. 1993. Characteristics of semi-conformable alteration zones associated with volcanogenic massive sulfide districts. *Journal of Geochemical Exploration* 48:175–200.

Gill J. B. 1981. *Orogenic andesites and plate tectonics.* Berlin: Springer-Verlag. 390 p.

Hannington M., Jonasson I. R., Herzig P. M., and Petersen S. 1995. Physical and chemical processes of seafloor mineralization at mid-Ocean ridges. In *Seafloor hydrothermal systems: Physical, chemical, biological, and geological interactions,* edited by Lupton J., Mullineaux L., and Zierenberg R. Geophysical Monograph 91. Washington D.C.: American Geophysical Union. pp. 115–157.

Ivanov B. A. and Deutsch A. 1999. Sudbury impact event: Cratering mechanics and thermal history. In *Large meteorite impacts and planetary evolution II,* edited by Dressler B. O. and Sharpton V. L. Special Paper 339. Boulder: Geological Society of America. pp. 389–397.

Kettrup B., Deutsch A., Ostermann M., and Agrinier P. 2000. Chicxulub impactites: Geochemical clues to the precursor rocks. *Meteoritics & Planetary Science* 35:1229–1238.

Kring D. A. and Boynton W. V. 1992. Petrogenesis of an augite-bearing melt-rock in the Chicxulub structure and its relationship to K/T impact spherules in Haiti. *Nature* 358:141–144.

Le Bas M. J., Le Maitre R. W., Streckeisen A., and Znnetin B. 1986. A chemical classification of volcanic rocks based on the total alkali-silica diagram. *Journal of Petrology* 27:745–750.

McCarville P. and Crossey L. J. 1996. Post-impact hydrothermal alteration of the Manson impact structure. Special Paper 302. Geological Society of America. pp. 347–376.

Molnar F., Watkinson D. H., and Jones P. C. 2001. Multiple hydrothermal processes in footwall units of the North Range, Sudbury igneous complex, Canada, and implications for the genesis of vein-type Cu-Ni-PGE deposits. *Economic Geology* 96:1645–1670.

Naldrett A. J. 2003. From impact to riches: Evolution of geological understanding as seen at Sudbury, Canada. *GSA Today* 13:4–9.

Naumov M. 2002. Impact-generated hydrothermal systems: Data from Popigai, Kara, and Puchezh-Katunki impact structures. In *Impacts in Precambrian shields,* edited by Plado J. and Pesonen L. J. Berlin: Springer-Verlag. pp. 117–172.

Pflumio C. 1991. Evidence for polyphased oceanic alteration of the extrusive sequence of the Semail Ophiolite from the Salahi Block (Northern Oman). In *Ophiolite genesis and evolution of the oceanic lithosphere,* edited by Peters T., Nicolas A., and Coleman R. G. Boston: Kluwer Academic Publishers. pp. 313–351.

Pilkington M. and Hildebrand A. R. 2000. Three-dimensional magnetic imaging of the Chicxulub crater. *Journal of Geophysical Research* 105:23479–23491.

Pilkington M., Ames D. E., and Hildebrand A. R. 2004. Magnetic mineralogy of the Yaxcopoil-1 core, Chicxulub crater. *Meteoritics & Planetary Science* 39:831–841.

Rogers D. F., Gibson H. L., Whitehead R., Checetto J., and Jonasson I. R. 1995. Structure and metal enrichment in the hanging wall carbonaceous argillites of the Paleoproterozoic Vermilion and Errington Zn-Cu-Pb massive sulfide deposits, Sudbury, Canada. *Geological Association of Canada-Mineralogical Association of Canada Program with Abstracts* 20:90.

Rousell D. H. 1984. Mineralization in the Whitewater Group. In T*he* *geology and ore deposits of the Sudbury structure,* edited by Pye E. Special volume 1. Ontario: Ontario Geological Survey. pp. 219–232.

Schuraytz B. C., Sharpton V. L., and Marin L. E. 1994. Petrology of impact-melt rocks at the Chicxulub multiring basin, Yucatán, México. *Geology* 22:868–872.

Spry P. G., Peter J. M., and Slack J. F. 2000. Meta-exhalites as exploration guides to ore. In *Metamorphosed and metamorphogenic ore deposits,* edited by Spry P. G., Marshall B., and Vokes F. M. Littleton: Society of Economic Geologists. pp. 163–201.

Steiner M. B. 1996. Implications of magneto-mineralogical characteristics of the Manson and Chicxulub impact rocks. In *The Cretaceous-Tertiary event and other catastrophes in earth history,* edited by Ryder G., Fastovsky D., and Gartner S. Special Paper 307. Boulder: Geological Society of America. pp. 89-104.

Vermeesch P. and Morgan J. V. 2004. Chicxulub central crater structure: Initial results from physical property measurements and combined velocity and gravity modeling. *Meteoritics & Planetary Science.* This issue.

Whitehead R. E. S., Davies J. F., and Goodfellow W. D. 1992. Lithogeochemical patterns related to sedex mineralization, Sudbury basin, Canada. *Chemical Geology* 98:87–101.

Zürcher L. and Kring D. A. 2003. Preliminary results on the post-impact hydrothermal alteration in the Yaxcopoil-1 hole, Chicxulub impact structure, Mexico (abstract #1735). 34th Lunar and Planetary Science Conference. CD-ROM.